Laue crystallography: coming of age

Zhong Ren,[a]* Dominique Bourgeois,[b,c] John R. Helliwell,[d] Keith Moffat,[a] Vukica Šrajer[a] and Barry L. Stoddard[e]

[a]*Department of Biochemistry and Molecular Biology and Consortium for Advanced Radiation Sources, The University of Chicago, 920 East 58th Street, Chicago, IL 60637, USA,* [b]*European Synchrotron Radiation Facility, BP 220, 38043 Grenoble CEDEX, France,* [c]*UPR 9015/IBS, 41 Avenue des Martyrs, 38027 Grenoble CEDEX 1, France,* [d]*Department of Chemistry, University of Manchester, Manchester M13 9PL, UK, and* [e]*Program in Structural Biology, Division of Basic Sciences, Fred Hutchinson Cancer Research Center, 1100 Fairview Avenue N. A3-023, Seattle, WA 98109, USA. E-mail: renz@cars.uchicago.edu*

A renewed interest in the Laue diffraction technique has been brought about by the development of new, more intense and brilliant synchrotron sources along with their insertion devices such as wigglers and undulators, and by the prospect of using these sources to study structural dynamics by time-resolved crystallography. Theoretical studies during the past decade have identified unique features of the polychromatic diffraction geometry and greatly improved our understanding of the Laue method. This led to innovative approaches to Laue data processing and its software implementation. Most of the problems in Laue data processing, considered for a long time to limit the applicability of the technique, have been solved. Significant advances have also been made in the development of synchrotron sources, beamline optics and instrumentation, and the X-ray detectors. Static Laue experiments yield structure amplitudes that equal those from monochromatic data in quality. When coupled with careful consideration of data-collection strategies and reaction initiation in crystals, a series of successful time-resolved Laue experiments on biological systems have been conducted. These have revealed information on structural dynamics inaccessible to any other conventional diffraction method. These static and time-resolved experiments demonstrate that the Laue method is coming of age. They also suggest avenues for future improvements: a correct treatment of finite mosaic spread and the associated energy width of Laue spots; consideration of diffuse scattering; and determination of intermediate structures in time-resolved experiments in which those intermediates do not attain a high concentration.

Keywords: Laue diffraction; time-resolved crystallography.

1. Introduction

What does it mean to state that an experimental technique is coming of age? Techniques evolve from a pioneering stage in which the qualitative observation of a phenomenon is itself noteworthy; through a more or less protracted development stage of experimental strategies, in which the sample, hardware and software factors that limit the quality, quantity and ease of acquisition of data by the technique are identified and refined, and artifacts eliminated or minimized; and towards a mature stage in which the technique is adopted by a wider range of practitioners and applied to a variety of scientific problems. In the recent history of macromolecular crystallography, this process is well illustrated by the evolution of the multiple-wavelength anomalous dispersion (MAD) technique, of virus crystallography, or of the molecular replacement technique.

In this overview we assert that the Laue technique in macromolecular crystallography has largely completed the second developmental stage: it has in that sense come of age. In support of this assertion we provide an overview of the main aspects of the Laue technique in §2 (principles), §3 (hardware) and §4 (software), with frequent reference to earlier articles; discuss the application scenarios of the Laue technique and several experimental considerations in time-resolved studies in §5; summarize the key static and time-resolved experimental results in §6; then point to ongoing and future developments to improve the Laue technique, to extend its range of applicability, and to drive it towards the third mature stage in §7.

It is no surprise that the chief area of application of the Laue technique to date, and a prime motivation for its development, lies in time-resolved studies (Ren & Moffat, 1994). We emphasize at the outset that in a time-resolved crystallographic experiment the essence of crystallinity,

translational symmetry, is lost. Although reaction initiation is designed to be effectively synchronized throughout the macroscopic volume of the crystal, results to date suggest that thereafter the molecules in the crystal behave independently of one another, just as if they were in dilute solution. That is, populations of intermediates rise and fall, governed by the rate constants for interconversion of structurally distinct species. Molecules do not march along the reaction coordinate in lockstep. Synchronicity is lost, which leads to the question posed by Ringe *et al.* (1992): can Laue catch Maxwell? The answer appears to be yes in particular cases, but developments outlined in §7 will have to be successfully explored before this can be stated with complete confidence.

2. Laue geometry

The Laue method is an X-ray diffraction method from single crystals that differs from the much more widely used monochromatic diffraction methods by utilizing, first, a stationary crystal and, second, the polychromatic X-rays naturally emitted by the synchrotron and its insertion devices. The Laue technique permits much shorter exposure times than monochromatic techniques by three to four orders of magnitude (Moffat, 1997). It is therefore ideally suited for time-resolved studies of structural changes in biological macromolecules 'at work' (Šrajer *et al.*, 1996; Perman *et al.*, 1998).

Fig. 1 is a simulated Laue pattern from a Flock House virus (FHV; Fisher *et al.*, 1992) crystal at an arbitrary orientation. Fig. 2 shows the Ewald construction illustrating Bragg's Law in reciprocal space. All reciprocal lattice points R between the minimum and maximum wavelengths (represented by the λ_{min} and λ_{max} spheres) and inside the resolution limit d_{min} sphere will yield diffraction rays. Each reflection is stimulated by a distinct wavelength (if the crystal mosaic spread is negligible; see §7.1 for consideration of the effects of finite mosaic spread). Therefore, the
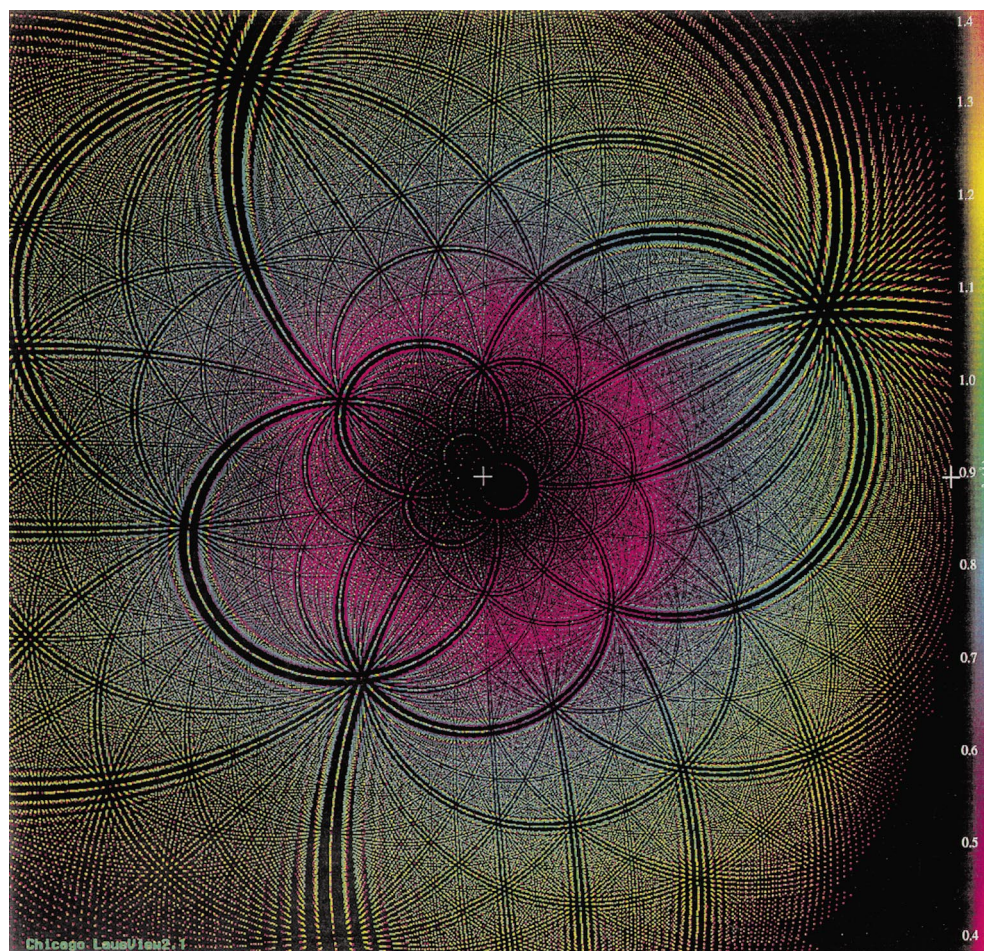

Figure 1
A simulated Laue diffraction pattern from a Flock House virus (FHV) crystal at an arbitrary orientation, recorded on a flat area detector. The crystal is in a rhombohedral space group with cell length $a = 325.5$ Å and cell angle $\alpha = 61.7°$ (Fisher *et al.*, 1992). The detector is inclined by 22.3° with an active area of 204.8 × 204.8 mm, at a crystal-to-detector distance of 250 mm. The highest resolution d_{min} is set at 3 Å and the wavelength range is 0.4–1.4 Å. Colours code the energies that stimulate the reflections. The crosses at the centre and the right edge of the image mark the direct-beam position and the perpendicular drop from the crystal centre to the detector surface, respectively. The image was generated by *LaueView* (Ren & Moffat, 1995a).

integrated intensity of each spot needs to be normalized at this wavelength prior to merging and averaging. This procedure is known as wavelength normalization, the outcome of which is denoted the λ-curve. The λ-curve is a mixture of the source spectrum, the diffraction efficiency factor $1/\lambda^2$, an overall absorption correction and the wavelength-dependent response of the detector. The spectrum of the X-ray source can be experimentally measured and/or determined from the diffraction data set (§3.1 and §4.3.3).

If a radial line OR (a central ray) in Fig. 2 passes through a single reciprocal lattice point R, a single reflection is recorded at the corresponding location on the detector. If a radial line passes through a series of reciprocal lattice points, these reflections are recorded cumulatively in the same location on the detector, which is called a multiple spot. Since the radial line between O and d_{min} spans an energy range, the overlap is denoted energy overlap. Since only harmonic reflections can lie on the radial line OR, the overlap is also denoted harmonic overlap. A comprehensive study on multiplicity distribution by Cruickshank et al. (1987) shows that no more than 17% of total reflections will be involved in energy overlap; that no single reflection can be possibly recorded at a resolution lower than $2d_{min}$ and a wavelength longer than $2\lambda_{min}$; and that single reflections have a higher probability of being located at higher Bragg angl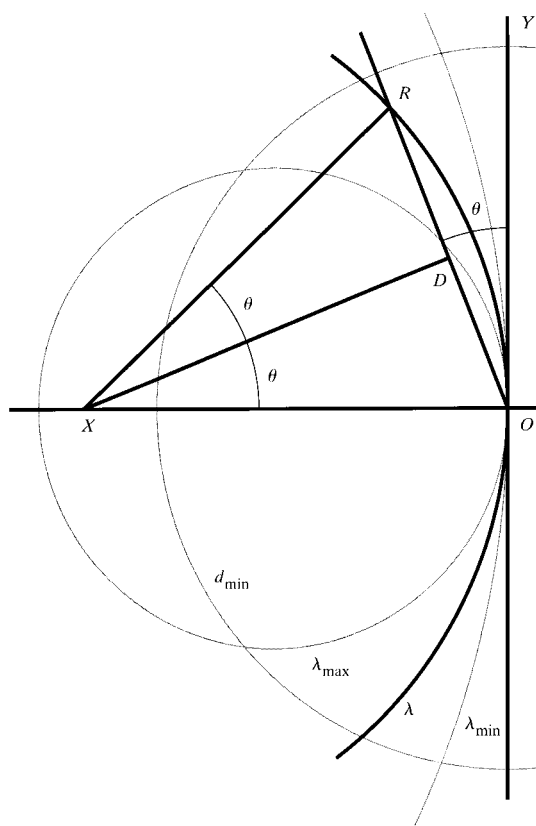es. The procedure to resolve multiple spots into their component reflections is known as harmonic deconvolution (§4.3.4).

Laue diffraction patterns are often crowded and contain many spatially overlapped spots (Figs. 1 and 3). Cruickshank et al. (1991) also demonstrated that the severity of spatial overlap is a function of Bragg angle; that severe spatial overlap is always one-dimensional, occurring along principal zones; and that spots with a high multiplicity (nodal spots) are surrounded by clear spaces (Fig. 3). Spatial overlaps need to be resolved during the spot integration procedure (§4.3.2).

During Laue data collection the φ-spacing between adjacent Laue images ultimately has great impact on the connectivity of the resultant electron density map (Ren & Moffat, 1995b; Bradbrook et al., 1997). The fraction of all reflections at a resolution d stimulated in a single Laue exposure with a wavelength range from λ_{min} to λ_{max} is $(\lambda_{max} - \lambda_{min})/2d$ (Moffat, 1997). Therefore, the spacing between successive spindle angles $\Delta\varphi$ during data collection should not exceed

$$\Delta\varphi_{max} = \pi(\lambda_{max} - \lambda_{min})/d \qquad (1)$$

if complete data are to be collected at resolution d. Notice that even when $\Delta\varphi_{max}$ is used, the data at resolution d are still far from complete. The accessible volume between the λ_{min} and λ_{max} spheres does not include two small conic spaces near the spindle axis, and the volumes accessible in successive exposures do not fit each other well. A more stringent estimate of $\Delta\varphi$ is possible that leaves no uncovered space between successive exposures but yields significant overlap,

$$\Delta\varphi_{min} = \sin^{-1}(\lambda_{max}/2d) - \sin^{-1}(\lambda_{min}/2d). \qquad (2)$$

Effective harmonic deconvolution procedures are then essential to realise the theoretical completeness at low resolution.

If an experimental φ-spacing is $\Delta\varphi$, the average redundancy r at resolution d is

$$r \geq \Delta\varphi_{max}/\Delta\varphi. \qquad (3)$$

The equality is met when $\Delta\varphi = \Delta\varphi_{min}$, and then

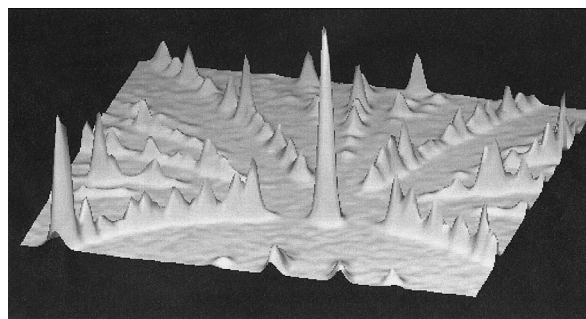$$r = \pi(\lambda_{max} - \lambda_{min})/d\,\Delta\varphi. \qquad (4)$$

Figure 2
Ewald construction of Laue geometry.

Figure 3
A three-dimensional surface representation of a Laue diffraction image near a nodal spot.

Fig. 4 shows the redundancy r as a function of resolution d, when $\Delta\varphi_{min}$ appropriate to that resolution is chosen. The value of r remains closely around 6 for the entire resolution range from 1 Å to infinity; and it can be shown (Z. Ren, unpublished results) that r is not strongly wavelength-dependent. When $\Delta\varphi_{min}$ is chosen, the data are barely complete at resolution d; the redundancy, however, is already above 6. This demonstrates that it is hard to collect complete Laue data sets, but easy to collect highly redundant data. Redundancy cannot be traded for completeness. This unique feature of Laue geometry provides a solid foundatio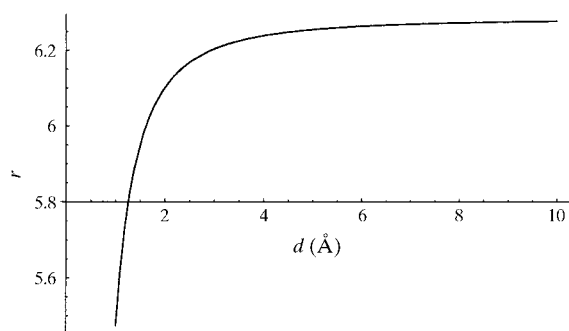n for several critical data-processing procedures such as wavelength normalization (§4.3.3) and harmonic deconvolution (§4.3.4).

The main advantage of Laue diffraction, very short exposures and hence very high time resolution, is set off against a number of difficulties. These are summarized in Fig. 5, and fall into two main categories: experimental relevance and data quality. The former includes whether a polychromatic X-ray beam perturbs the crystal, and whether the Laue technique is yet fast enough to study irreversible reactions; the latter addresses whether very rapid Laue data collection yields well behaved Fourier maps, and whether the accuracy and the achievable resolution of Laue data are adequate to cope with subtle structural modifications occurring on short timescales. Fig. 5 clearly shows that answers to these questions largely depend on crystal quality and on the performance of the X-ray source, optics and detector. Assuming that adequate crystals have been prepared and that optimized instrumentation is available, the success of a Laue experiment will depend on the choice of a wise data-collection strategy (Yang *et al.*, 1998), and on effective use of Laue data-processing packages (Clifton *et al.*, 1997).

Figure 4
Laue data redundancy r at resolution d [equation (4)] with $\lambda_{max} = 1.3$ Å and $\lambda_{min} = 0.3$ Å.

3. Laue beamlines

Synchrotrons provide ideal X-ray sources for Laue diffraction experiments: they are polychromatic, intense
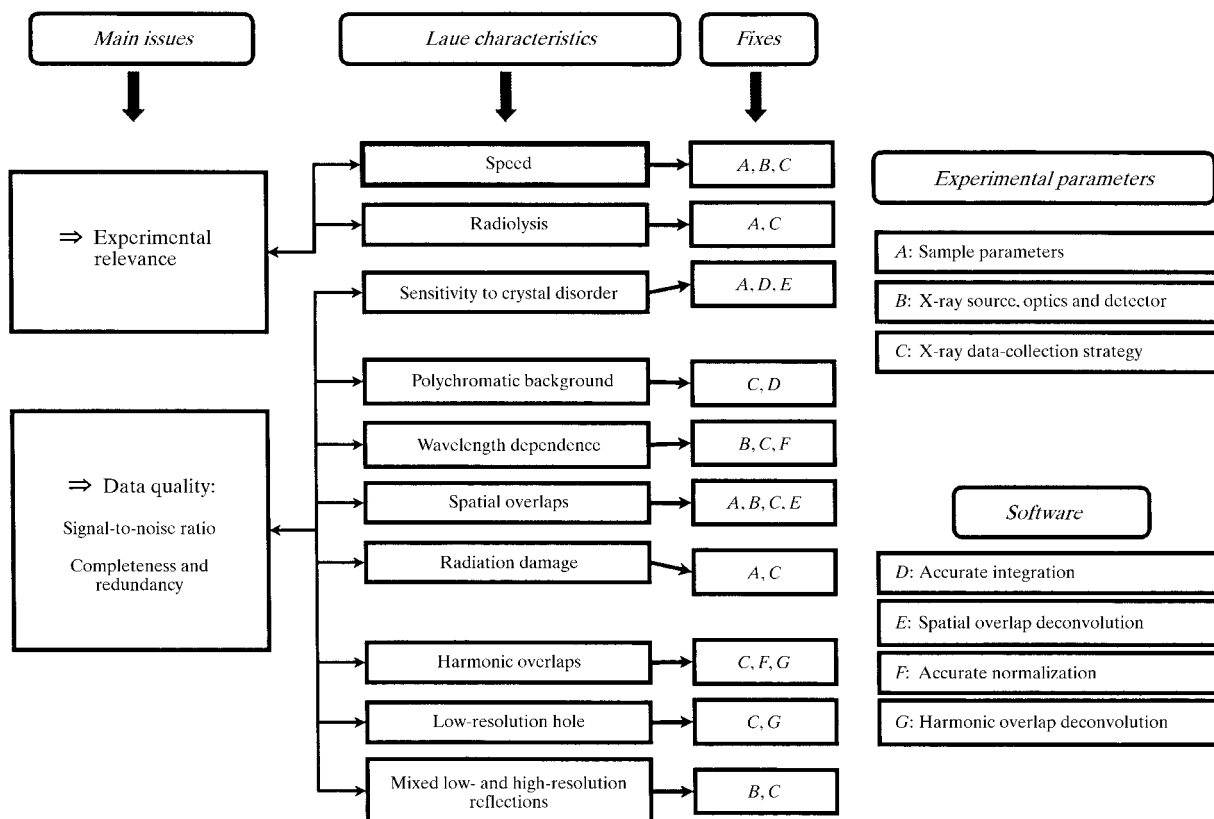

Figure 5
Major issues involved in Laue geometry and its applications.

and pulsed (Helliwell, 1997). The first is intrinsic to the radiation emission process; the second and third allow a further reduction in the X-ray exposure times that are already several orders of magnitude shorter than those needed for monochromatic experiments. To achieve the very short exposure times needed for time-resolved experiments, it is important to select the X-ray source and optimize the optics so that the maximum power density is delivered to the sample as a well focused and stable X-ray beam. High-brightness insertion devices (wigglers and undulators) are necessary for sub-μs exposure times, while bending magnets are well suited when μs to s exposure times are sufficient. However, even at third-generation synchrotron sources, the ultrafast time-resolved studies with exposure times of ∼100 ps (the duration of a single X-ray pulse; Bourgeois et al., 1996) require a 10 to 100 fold increase in X-ray intensity, if averaging by multiple exposures is to be avoided for typical size crystals (e.g. 200 μm). This at present restricts the application of these types of ultrafast experiments to reversible reactions only (Moffat, 1998a,b). Progress in synchrotron radiation technology or the development of free-electron lasers at hard X-ray wavelengths may improve the situation in the future.

Several beamlines have been designed and constructed specifically for use of the Laue technique on biological macromolecules. They include the X26C beamline at the National Synchrotron Light Source (NSLS), Brookhaven National Laboratory, USA (http://www.nsls.bnl.gov/Beam-Line/pages/x26c.html); the ID09 beamline at the European Synchrotron Radiation Facility (ESRF), France (http://www.esrf.fr/exp_facilities/ID9/handbook/handbook.html); the 14-ID and 14-BM beamlines at the Advanced Photon Source (APS), Argonne National Laboratory, USA (http://cars.uchicago.edu) and the BL44B2 beamline at SPring-8, Japan (http://www.spring8.or.jp/ENGLISH/facility/bl/RIKENBL/BL44B2/index.html). Experimental details are discussed by Moffat (1997) and references therein.

3.1. Spectral properties

The spectral properties of the X-ray radiation delivered to the crystal and sensed by the detector, such as the bandpass (λ_{max} to λ_{min}) and the shape of the X-ray spectrum, have to be considered when choosing the right source and optics for Laue experiments. These properties are in practice determined by a choice of the source (bending magnet, wiggler or undulator), by the mirror coating and grazing angle, and by inserting multilayer devices and various filters into the beam.

In general, shorter wavelengths provide the advantage of reduced radiation and thermal sample damage. Absorption effects, which are difficult to fully correct by data processing software, are also reduced. However, the efficiency of most detectors diminishes at shorter wavelengths. Results on Laue data processing suggest that the wavelength range of 0.4–1.8 Å (7–30 keV) is acceptable (Helliwell, Habash et al., 1989; Šrajer et al., 1996; Yang et al., 1998; Genick et al., 1997).

The choice of an adequate spectral bandpass is crucial (Sweet et al., 1993). A relatively narrow bandpass reduces the number of harmonic and spatial overlaps and the polychromatic background. Laue patterns are therefore less crowded and the signal-to-noise ratio should be improved. However, the narrow bandpass requires a larger number of frames to be collected for a complete Laue data set (§2), and frame-to-frame scaling errors may be enhanced. In time-resolved experiments with reversible photosensitive systems where each X-ray exposure is preceded by a laser exposure, a larger number of frames requires a larger number of potentially damaging laser pulses to be delivered to the sample. In irreversible reactions, each repeated reaction initiation necessary to complete a data set might require a new crystal. Clearly, in both cases a smaller number of frames is desirable. Narrow-bandpass insertion devices such as the single-line U20 undulator at the ID09 beamline at ESRF present additional challenges for the data-processing software. A significant fraction of data becomes partial, especially at low resolution (see §7.1 for details), and spectra exhibit a particularly sharp intensity variation with wavelength. The former problem is not addressed by the existing data-processing software. The latter can, however, be successfully handled by software, as demonstrated by processing of Laue data collected at the ID09 beamline using various insertion devices (Šrajer et al., 1999). The U26 and U20 undulator spectra, as well as the complex spectrum of the W70 wiggler and U46 undulator used in series, have been successfully derived from the data using high-degree Chebyshev polynomials to model the sharply varying wavelength-normalization curve in LaueView (Ren & Moffat, 1995a).

It might be particularly advantageous to use single-line undulators for reversible reactions, provided that the crystal can sustain repeated reaction initiation and that progress is made in treating partials by the data-processing software. The smooth wide-bandpass spectra and high X-ray flux afforded by wigglers make them proven reliable sources for reversible systems (Šrajer et al., 1996; Perman et al., 1998) and the source of choice for irreversible systems. However, these advantages occur at the expense of a somewhat decreased signal-to-noise ratio due to their higher background compared with undulators.

3.2. Exposure time control

A fast X-ray shutter is necessary to accomplish the short exposure times in Laue experiments. Single-opening X-ray shutters, such as an electromagnetically driven tungsten blade that moves in and out of the X-ray beam, are typically limited to opening times of ∼1 ms. The opening times of rotating X-ray shutters such as a channel-cut rotating disc can reach 1–2 μs (LeGrand et al., 1989; Bourgeois et al., 1996; Wulff et al., 1997). An additional millisecond shutter can be used in series with a rotating shutter when it is desirable to isolate a single opening of the rotating shutter which typically occurs every 1–3 ms. Such a shutter train was used in the nanosecond time-resolved Laue experi-

ments on the ID09 beamline (Bourgeois *et al.*, 1996; Šrajer *et al.*, 1996; Perman *et al.*, 1998). The rotating shutter was synchronized with the X-ray clock to pass one 150 ps X-ray pulse per opening in the single-bunch operating mode of the storage ring, and the millisecond shutter was used to isolate only one opening of the rotating shutter. This sequence was repeated as necessary for signal averaging, but the time interval between successive X-ray exposures was of the order of several seconds. These deliberately long intervals were necessary to allow full reversal of structural changes produced by the laser pulse arriving prior to the X-ray pulse, and dissipation of energy (heat) deposited in the crystal by the laser pulse.

3.3. Detectors

In considering which detector should be used for Laue data collection, the important factors are largely the same as for monochromatic data collection: dynamic range, detective quantum efficiency (DQE), size, point spread function, energy response, readout time, readout noise and dark current. A large dynamic range is desirable (perhaps even more so in Laue experiments than in monochromatic) due to the large variation in incident X-ray intensity with wavelength. The detector should be large in active area, both to record the reflections at higher resolution stimulated by longer wavelengths in the X-ray spectrum and to accommodate the larger crystal-to-detector distances desirable to minimize spatial overlaps. The point spread function must be sufficiently small not to worsen the spatial overlap problem. A high DQE in the energy bandpass of interest is of particular importance in time-resolved experiments that generate weak diffraction patterns from the quite short exposures. It is also desirable that the DQE varies with the X-ray dose; it should be high when the X-ray dose is low. A low readout noise enhances the signal-to-noise ratio for weak reflections. However, a low dark current is not critical since Laue exposures are very short; but it becomes essential when the signal is averaged by collecting multiple exposures at the detector prior to readout. A fast readout improves the Laue experiment duty cycle, since the readout time is always much longer than the very short Laue exposure times. A fast readout is critical when an irreversible reaction is followed after a single reaction initiation, since the time resolution in this type of experiment is actually restricted by the detector readout time. Finally, the energy response of the detector and its dependence on wavelength and obliquity have to be considered and appropriate corrections applied to data. A careful calibration of detectors used for Laue data collection at various energies still remains to be performed.

Both image-plate (off- and on-line) and CCD detectors have been successfully used for Laue data collection. The advent of automatic readout of these detectors *versus* the early days of the synchrotron Laue method with film have hugely changed the capacity to record many orientations for multiple Laue exposures from the crystal. Thus completeness and redundancy (§2) have been greatly facilitated for Laue data sets. Moreover, the improved DQE of these detectors allows shorter exposures to the sample for a given data accuracy and thus more exposures to be recorded before the sample decays.

4. Laue data collection and processing

In this section we review the main characteristics of the Laue technique in terms of three closely related aspects: crystal parameters, data-collection strategy and data processing.

4.1. Crystal parameters

The success of a Laue experiment is primarily determined by the crystal conditions (denoted A in Fig. 5). Some crystals may be altered by radiolysis effects that produce undesirable side reactions. Others show unacceptable disorder during the course of a structural reaction. Yet others are simply too fragile to withstand the considerable radiation dose delivered during an extended white or pink beam exposure. (In a pink beam, higher-energy X-rays are removed from the white beam by total external reflection from a mirror.) The necessary exposure may then have to be delivered as a set of sub-exposures (Moffat, 1997). Moderate cooling of crystals is likely to be beneficial, but cryocooling is not a solution since a main interest of Laue experiments is in the study of macromolecules at near physiological temperature where molecular motion associated with structural reactions is retained, not frozen out. High-symmetry space groups are advantageous since they will reduce the minimum number of frames needed to collect a complete data set. However, crystal selection will always be largely driven by the scientific questions posed in structural biology.

4.2. Data-collection strategy

Once promising crystals and an appropriate Laue experimental station are available, the data-collection strategy must be thought through carefully. It is usually best to use a coarse $\Delta\varphi$ first [such as $\Delta\varphi_{max}$ in equation (1)], and then to fill in the gaps by several passes until $\Delta\varphi_{min}$ in equation (2) is achieved. This strategy yields more uniform sampling of reciprocal space even when radiation damage is a problem and $\Delta\varphi_{min}$ cannot be achieved.

The best results can only be obtained when crystal parameters, source parameters, data-collection strategy and data-processing ability are considered together. For example, the choice of the crystal-to-detector distance is closely related to the maximum cell length, crystal diffraction limit, detector size and X-ray wavelength range. The necessity to minimize spatial overlaps and to cover a sufficiently high Bragg angle needs to be considered jointly. The ability of software to resolve spatial overlaps has a great influence on the choice of crystal-to-detector distance. Sometimes it may be desirable to shift the detector off axis to cover higher Bragg angles. A two-pass exposure strategy was successfully used to compensate for

the limited dynamic range of the detector in a high-resolution Laue data collection from restrictocin (Yang *et al.*, 1998). The first low-resolution pass used 0.5 ms of exposure per image; the second high-resolution pass used a 10 ms exposure. The first pass used a centred detector; the second used a shifted detector. A toast-rack arrangement of films was proposed to deal with factors such as spatial overlap, energy overlap, detector dynamic range and Bragg-angle acceptance (Helliwell, 1991). However, this strategy is restricted to largely transparent detectors such as film and has not been widely used with the arrival of non-transparent image-plate and CCD detectors.

The signal-to-noise ratio in Laue diffraction patterns in time-resolved experiments can be poor because of the higher-level polychromatic background and the limited X-ray flux when a very short exposure time is to be achieved, as in single-bunch experiments (Bourgeois *et al.*, 1996). To remedy this problem, one could limit the X-ray background by reducing the X-ray bandpass, for example, by utilizing a multilayer or a single-line undulator, and seek to increase the diffracted signal by increasing the synchrotron ring current. A more frequently adopted strategy is to average multiple exposures under identical conditions on each image when studying a reversible reaction (Šrajer *et al.*, 1996; Perman *et al.*, 1998). Such averaging takes place at the same delay time after reaction initiation, when the fractional concentration for each intermediate reaches the same value.

4.3. *Data processing*

Data processing concentrates on efficient extraction of signal and suppression of error (Clifton *et al.*, 1997). A flow chart of typical Laue data processing is presented in Fig. 6. As in the more familiar monochromatic data processing, it consists of three major parts: geometric prediction of diffraction patterns, integration of diffraction spots, and data reduction. Laue data reduction includes wavelength normalization, frame-to-frame scaling, and harmonic deconvolution. Efficient software packages were developed for this purpose, including *LaueView* (Ren & Moffat, 1995*a,b*) and the Daresbury Laue Software Suite (Helliwell, Habash *et al.*, 1989; Campbell, 1995). Improvements to specific parts of the processing were proposed: *LEAP* (Wakatsuki, 1993), *Lauecell* (Ravelli *et al.*, 1996; Ravelli, 1998), *PrOW* (Bourgeois *et al.*, 1998), and other implementations based on Bayesian theory (Bourenkov *et al.*, 1996; Ursby & Bourgeois, 1997).

4.3.1. *Indexing and geometry refinement.* The first step in 'modern' Laue data processing consists of indexing diffraction patterns from crystals whose orientation matrix is unknown (in the 'old days', crystals were often manually pre-oriented!). In most practical cases, cell parameters are accurately known from previous monochromatic experiments and only the crystal orientation needs to be determined. This can be efficiently achieved with packages like *LaueView* (Ren & Moffat, 1995*a*) or *Lauegen* (Campbell, 1995), using the method of Helliwell, Habash *et al.* (1989).

In this method, two series of interplanar angles are calculated in reciprocal space, the first using a few (nodal) spots selected from the experimental Laue pattern, and the second using the known reciprocal Bravais lattice. The orientation matrix of the crystal is obtained by comparing and matching these two lists. Accurate evaluation of experimental interplanar angles necessitates correct identification of the direct-beam centre. This can be achieved during the Laue experiment by using a semi-transparent beamstop or later by software, by computing the point of intersection between several Laue conics in the diffraction pattern

When cell parameters are not known, other indexing methods are able to determine the crystal orientation and the relative cell dimensions. They rely on the use of the gnomonic projection (Carr *et al.*, 1992), or on a recognition of conics by a plane search algorithm in reciprocal space (program *Lauecell*; Ravelli *et al.*, 1996). The determination of absolute cell dimensions requires the identification of a known wavelength in the X-ray spectrum, to introduce a length scale. This may, for example, be performed by inserting a metal foil with a known absorption edge into the beam (Carr *et al.*, 1993), or by identifying one characteristic edge from a mirror coating in the beamline optics. A useful review on Laue indexing can be found by Ravelli *et al.* (1999).

Even in the common case where cell parameters are known to good accuracy, the ease of indexing a Laue pattern relies on a favourable crystal orientation for the
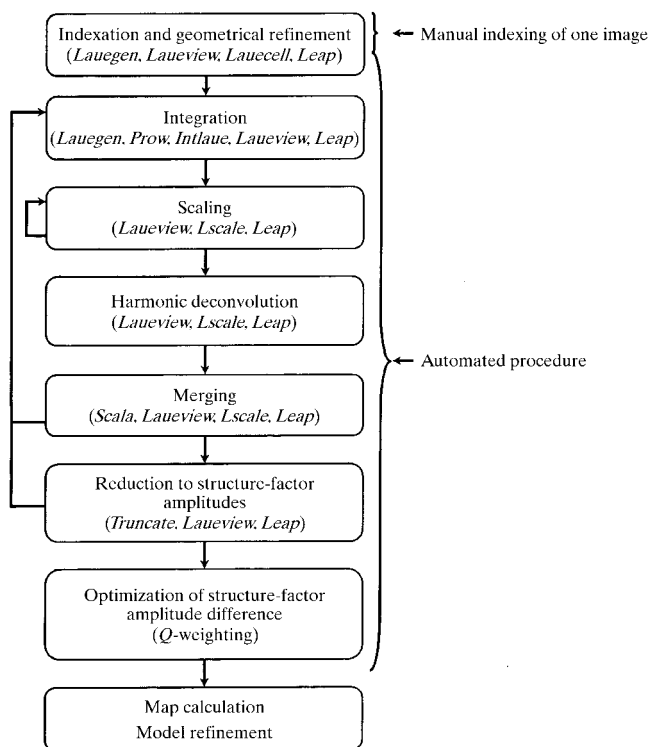

Figure 6
Flow chart of typical Laue data processing.

image being worked on. Some images in a complete data set are easier to index correctly than others. These images usually show elliptical rather than parabolic or hyperbolic conics, and are characterized by a number of clearly identifiable nodal spots where prominent conics intersect.

Pattern indexing is followed by determination of the effective X-ray wavelength range and the resolution limit. Histograms of the ratio $I/\sigma(I)$ can be computed to assess the short wavelength limit λ_{min} and the resolution limit d_{min} (Hao *et al.*, 1995; Ren & Moffat, 1995a). The long wavelength limit λ_{max} is more difficult to determine, and may be established from the knowledge of experimental parameters (such as the presence of attenuators in the beam) and inspection of the patterns. In practice, there are no 'hard' limits of wavelength and resolution in Laue patterns, and soft boundaries should be used instead. A resolution-dependent spectral bandpass, or wavelength-dependent resolution limit, implements soft rather than hard limits on d_{min}, λ_{min} and λ_{max}. This scheme permits dynamically adjusting these soft limits based on Wilson statistics (Wilson, 1942) and prior knowledge of the source spectrum (§3.1). Fig. 7 shows the probability distribution of measurable reflections in reciprocal space. Let d_{min} be the very highest resolution where reflections are barely measurable at the peak of the X-ray spectrum. Such reflections will not be measurable at the two wings and other weak regions of
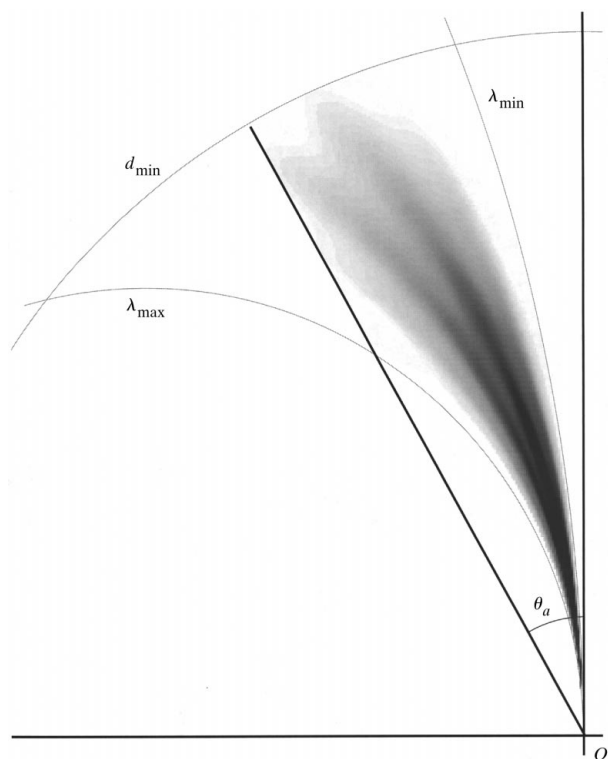

Figure 7
Probability distribution of measurable reflections in reciprocal space. A λ-curve of beamline ID09 with a wiggler W70/undulator U46 source at the ESRF is used. Darker grey levels indicate higher probability.

the spectrum. The lowest contour line defines a new accessible region that replaces the region defined by the three spheres of d_{min}, λ_{min} and λ_{max}. *LaueView* includes an implementation of a resolution-dependent bandpass. This technique is of key importance when dealing with sharply varying X-ray sources like undulators (Bourgeois *et al.*, 1999).

Various conclusions need to be re-examined under the assumption of a resolution-dependent spectral bandpass compared with those based on hard limits. First, a lower completeness and redundancy can be realistically achieved than those theoretically predicted with hard limits, especially at higher resolution and, therefore, a finer angular spacing $\Delta\varphi$ should be employed in data collection. However, at low resolution, predicted completeness and redundancy described above are little affected; completeness and redundancy at low resolution are still the concern. Second, software which implements a resolution-dependent bandpass allows a more optimistic setting of soft limits and should also tolerate larger errors in these settings, and requires less computation for spot integration. Third, fewer spatial overlaps truly exist than predicted from hard limits. Spot density distribution is less strongly dependent on Bragg angle than previously projected (Cruickshank *et al.*, 1991). Fourth, a better estimate for the Bragg angle acceptance θ_a can be carried out, if the spectrum is known when planning data collection. Fifth, fewer single reflections at high resolution, stimulated by longer wavelengths, can be realistically measured. Sixth, fewer energy overlaps exist, mainly due to the fact that data at high resolution, stimulated by short wavelengths, are not truly measurable. This liberates some reflections at a resolution lower than $2d_{min}$ and wavelength longer than $2\lambda_{min}$ from being harmonically overlapped. For a typical smooth bending-magnet or wiggler spectrum, energy overlap is reduced to about 13% from 17% (Z. Ren, unpublished results). Seventh, the discontinuity in data density at wavelength $2\lambda_{min}$ is removed. The λ-curve can be derived as a single curve with no discontinuity at $2\lambda_{min}$, even for high-resolution data sets (Ren & Moffat, 1995a).

Geometrical refinement of the calculated spot positions must also be performed in order to account for various imperfections of the instrumental system. Refinable parameters include crystal orientation matrix, crystal-to-detector distance, direct-beam position, tilt, twist, bulge and raster-shape of the detector and (some of) the cell dimensions, as well as various cross terms (Ren & Moffat, 1995a; Campbell, 1995). Geometrical refinement is usually achieved by least-square minimization between calculated and observed spot positions. The performance relies on the ability to precisely localize experimental spots, which proves more difficult when the Laue spots are weak, spatially overlapped or significantly elongated. Several refinement cycles should be applied, preferably with a limited number of well defined experimental spots rather than with a large number of unreliable spots, especially in the earlier passes. The root-mean-square deviation

between observed and calculated spot positions should (as a rule of thumb) not exceed half the raster size.

It is good practice to cycle geometrical refinement and determination of the X-ray wavelength range and resolution limit a couple of times, at least when processing the early images of a data set. However, once geometrical refinement is completed, it is wise to slightly over-predict the patterns, provided that subsequent software is able to cope with the resulting complications. Indeed, under-prediction may not only result in losing potentially useful information, but also in mis-assigning multiples and introducing bias into wavelength normalization.

4.3.2. *Integration.* Laue data integration is usually based on variants of the spot profile-fitting technique originally introduced by Rossmann (1979). Successful integration by profile fitting relies on four key aspects: accurate subtraction of X-ray and detector background; definition of high-quality model profiles that are used to fit weak and/or overlapped diffraction spots; proper determination of suitable fitting masks; and accurate evaluation of the integrated intensities from weak and/or overlapped spots and of their associated error estimates by least-square minimization. Non-overlapped strong spots can be accurately integrated by summation techniques. Other features, such as the possibility to reject obvious outliers or to mask out unreliable parts of the image, are also helpful (Shrive *et al.*, 1990; Wakatsuki, 1993; Greenhough & Shrive, 1994; Ren & Moffat, 1995*a*; Campbell *et al.*, 1998; Bourgeois *et al.*, 1998).

Deconvolution of spatially overlapped spots by software is crucial since there is no experimental solution that can completely eliminate such spots. The recent Laue integration programs are all designed to implement such deconvolution algorithms. Differences between them relate primarily to the construction of reference profiles and profile-fitting masks. In *LaueView* (Ren & Moffat, 1995*a*; Ren *et al.*, 1996), reference profiles are constructed analytically from a library built from well defined strong non-overlapped and accurately predicted spots in various detector bins. Analytical parameters defining the profile shape are derived from these spots and vary smoothly throughout detector space. Weak and/or overlapped spots whose shapes may vary due to radial elongation or anisotropy can be faithfully modelled. This technique has the advantage that it is not affected by detector sampling effects, since model profiles can be calculated at the predicted positions of the spots under evaluation. Due to the limited flexibility of analytical models, certain unusual spot shapes such as double-peaked spots may not be correctly evaluated. In *LaueView*, profile fitting is performed by least-square minimization over a fitting mask inscribed within an arbitrarily defined contour level of the model profile. The level of that contour does not depend on the signal-to-noise ratio of the spot under evaluation.

A different approach is used in *PrOW* (Bourgeois *et al.*, 1998). 'Learned' model profiles are constructed numerically from well behaved reference spots located in the vicinity of the spot under evaluation. Efficient procedures ensure that reference spots, which are selected based on severe criteria, are uniformly distributed throughout detector space. Fitting masks are also defined as areas inscribed within certain contour levels of the model profiles. However, the level of the contour depends on a prior estimate of the signal-to-noise ratio of the spot under evaluation. This dynamically adjusted profile-fitting area significantly improves the accuracy of the evaluation of weak diffraction spots, which are frequent in Laue patterns. This technique also allows the efficient flagging of spots as overlapped (Bourgeois, 1999).

Estimation of error associated with the integrated intensity is essential to the later success of wavelength normalization and data scaling. Two strategies are commonly used. An empirical approach is based on the profile-fitting residual (*LaueView*), which accounts in a reasonable manner for other types of errors which are difficult to model, *e.g.* errors resulting from positional inaccuracy in geometry refinement, or in digitization of the diffraction pattern. The error estimates eventually need to be calibrated from the variance of redundant data. The second approach is based on error propagation from the expression describing profile-fitted integrated intensities (*PrOW*). It is theoretically more elegant, but tends to neglect the contribution of systematic errors which in general become more pronounced for higher intensities. When such an approach is chosen, wavelength-dependent effects have to be taken into account. For example, the wavelength dependence of the detector gain must be included in estimation of variances, which is non-trivial in the case of a polychromatic background. A combined use of the two strategies might improve the reliability of error estimation.

4.3.3. *Wavelength normalization and data scaling.* Laue intensities are strongly modulated by various physical parameters, which need to be accounted for before usable structure factor amplitudes can be extracted. Data normalization is one of the most complex tasks of Laue data processing, since some of these parameters show a sharp wavelength dependence and may be correlated. A few improvements in numerical analysis and optimization of large-scale non-linear least-squares problems were recently carried out in *LaueView* (Ren *et al.*, 1999). Parallel implementation of the non-linear least-squares minimization is also available (Ren *et al.*, 1999).

The overall scale factor to be applied to integrated intensities can be expressed as (Ren & Moffat, 1995*a*):

$$f_{\text{overall}} = f_L f_P f_\lambda f_{\text{iso}S} f_{\text{iso}B} f_A f_{\text{aniso}S} f_{\text{aniso}B} f_{\text{iso}D} f_{\text{aniso}D} f_U f_O, \quad (5)$$

where f_L is the Lorentz factor ($= \sin^2\theta$), f_P accounts for the polarization ratio, $f_{\text{iso}S}$, $f_{\text{iso}B}$, $f_{\text{aniso}S}$ and $f_{\text{aniso}B}$ are isotropic and anisotropic inter-image scale and atomic displacement factors, f_λ is the wavelength-normalization factor, f_A is a general absorption correction, $f_{\text{iso}D}$ and $f_{\text{aniso}D}$ relate to potential radiation damage, and f_U and f_O correct for detector non-uniformity of response and non-linearity. An obliquity correction, accounting for the effect of a protec-

tive layer placed in front of the detector, may also be added (Arzt *et al.*, 1999). Most of these factors (f_L, f_P, f_{isoS}, f_{isoB}, f_{anisoS}, f_{anisoB}, f_{isoD}, f_{anisoD}) are not specific to the Laue technique and may in principle be handled as in the monochromatic case. The detector-dependent corrections f_U and f_O are usually applied to raw images prior to Laue data processing. Although these corrections should be wavelength-dependent (*e.g.* uniformity of detector response is usually strongly wavelength-dependent), they are generally applied as though they were wavelength-independent, in which a single wavelength is chosen close to the peak of the X-ray spectrum. This over-simplification may degrade results obtained with curved detectors, such as the image-intensifier detectors used at the ESRF.

The most critical normalization terms are f_λ and f_A. The factor f_λ accounts for variations in the X-ray spectrum as seen by the detector, and therefore gathers a series of various modulations (X-ray source, beamline optics, detector) which are difficult to accurately model by theory. There are two main approaches to deriving f_λ. The first consists of taking advantage of the structure factor amplitudes derived from a previously recorded monochromatic data set. This technique is neither the most elegant nor the more general. However, considering that the Laue technique is most often used to study transient structural states, where structure factor amplitudes differ only slightly from native amplitudes (which in the majority of cases are accurately known from a previous monochromatic experiment), this technique might be extremely efficient. Alternatively, the normalization curve can be evaluated by comparison of the intensities of symmetry-related reflections measured several times at different wavelengths, preferably in the same data set. The success of this technique depends on the naturally high redundancy of Laue data (§2). A so-called wavelength-binning method was initially proposed by Helliwell (1992) and implemented in the Daresbury Laue Software Suite (Campbell *et al.*, 1986; Helliwell, Habash *et al.*, 1989; Campbell, 1995). In this method a series of numbers representing the average value of the normalization curve within a small wavelength range is derived. A polynomial is then fitted to these numbers to yield an approximate λ-curve. Due to the limited number of bins that can be handled, the efficiency of this technique is diminished when the X-ray spectrum shows sharp features, for example, due to absorption edges from mirrors or detectors, or when an undulator source is used. To improve the accuracy of wavelength normalization, Ren & Moffat (1995a) followed the idea of Smith Temple (1989) and used Chebyshev polynomials to precisely model the λ-curve in *LaueView* [see Fig. 9 of Ren & Moffat (1995a) and Fig. 1 of Yang *et al.* (1998) for examples]. The choice of the degree of the polynomial has to make a compromise between the ability to accurately recover genuine sharp features of the X-ray spectrum and the tendency to fit noise. As an example, normalization of Laue data collected at the ESRF ID09 beamline recovered sharp spectral features present in the spectra of the undulators U20, U26 and combined

wiggler W70/undulator U46, by using Chebyshev polynomials of high degree up to 128 (Šrajer *et al.*, 1999).

Recently a similar technique for wavelength normalization, also based on using Chebyshev polynomials, was proposed by Arzt *et al.* (1999). In addition, an elegant way of correcting for absorption dependence of the integrated intensities [factor f_A in equation (5)] is proposed. The diffracted signal transmitted through a pathlength t is expressed by

$$T = V^{-1} \int_V \exp[-\mu(\lambda)t]\, dv, \qquad (6)$$

where V is the crystal volume. Whereas the wavelength dependence of the linear absorption coefficient μ may be accurately assessed from a relatively simple analytical model and from the knowledge of the sample composition, the pathlength t is more difficult to derive since it depends on the crystal shape and orientation for each diffracted ray. Arzt and co-workers estimate the effective pathlength t by using the concept of a general pathlength, which is modelled by two-dimensional Chebyshev polynomials (Ren & Moffat, 1995a). With this method the variation of t can be established at once throughout reciprocal space and applied individually for each reflection. However, this global general pathlength has to be broken down to an image-wide or orientation-specific function (Ren & Moffat, 1995a), when the crystal is not completely bathed in the X-ray beam.

The order in which the scaling parameters in equation (5) are refined is more or less a question of (careful) taste. In particular, one has to take care to prevent over-compensation effects. Compulsory corrections are f_L, f_P, f_{isoS}, f_{isoB}, f_λ, but other corrections dealing with absorption, anisotropy or radiation damage may significantly improve the final data quality. It is also important to note that reflections which at first appear to be outliers may turn out after parameter refinement not to be. This means that the overall scaling procedure and rejection of outliers should in general be cycled several times, possibly in an automated manner, until a number of quality indicators show satisfactory scores (Ren & Moffat, 1995a). The numerical quality indicators, such as the merging R-factor, are useful, and some graphical quality indicators, such as various error scatter plots, are often extremely sensitive to potential problems in data scaling [for example, see Fig. 5 of Ren & Moffat (1995a)].

Finally, when a Laue experiment is conducted in order to find out subtle structural differences between two closely related structures, it is preferable to normalize the two data sets together, and only separate the contributions from each once the data are properly scaled.

4.3.4. *Deconvolution of multiples.* Poor completeness of Laue data at low resolution is the origin of poor connectivity in Fourier maps, which often makes the interpretation of (difference) Fourier maps suspect. This difficulty can be substantially alleviated by deconvoluting the harmonic overlaps or multiples.

A variety of techniques have been proposed to retrieve the individual components of multiple spots. Experimental tricks to take advantage of the wavelength-dependent penetration of X-rays were proposed to stack several photographic films behind each other (Helliwell, Harrop *et al.*, 1989); or to repeated Laue exposures with a series of attenuators (Hanley *et al.*, 1996). Techniques based on direct methods (Hao *et al.*, 1993) or on Bayesian statistics (Bourenkov *et al.*, 1996; Xie & Hao, 1997) have the advantage of not relying on heavily redundant data. Deconvolution of multiples by making use of the normalization curve and data redundancy was shown possible by Campbell & Hao (1993). Robust procedures have been implemented in *LaueView* by Ren & Moffat (1995*b*), and recently in *LSCALE* (Arzt *et al.*, 1999). In this technique (which shows similarity with some de-twinning methods) individual contributions to multiple spots are retrieved by solving sets of linear equations. Normal matrices are essentially built from λ-curve coefficients, hence the accuracy of the deconvolution depends heavily on accurate wavelength normalization. In addition, a sufficient number of observations are necessary to provide an over-determined system, which implies the need for high data redundancy and the use of all available data across the available X-ray bandpass (§2). The efficiency of the deconvolution is greatly improved if observations from singles (possible multiples; Ren & Moffat, 1995*b*) are included in the sets of linear equations, and if the sets of equations that are linear in the intensities are converted to near-linear by substitution of the (squared) structure factor amplitude for the intensity (Ren & Moffat, 1995*b*).

4.3.5. *Optimization of difference Fourier maps.* Difference Fourier maps and difference refinement (Terwilliger & Berendzen, 1995, 1996) are often used to detect and investigate small conformational changes. Despite all the efforts in data processing, the noise in the difference structure factor amplitude ΔF may still be large compared with the signal. In time-resolved experiments the intrinsic signal-to-noise ratio can be very low since conformational changes are often limited in extent and intermediate structural states may be of low occupancy. Bayesian techniques, which essentially add relevant *a priori* information to experimental data, are valuable tools to ensure statistically correct distributions for experimental data. In the *q*-weighting technique (Ursby & Bourgeois, 1997) it is assumed that experimental measurements of structure factor amplitudes F_1 and F_2 are normally distributed around the true value F_{true}, and that the ensemble of ΔFs follows a Wilson distribution. The width of the distribution relates to the 'distance' between the related structures, and can be inferred from the data itself. With these assumptions, $\Delta F = F_1 - F_2$ for non-centrosymmetric reflections can be weighted by the factor q,

$$q = \sigma_D^2 / [\sigma_D^2 + 2(\sigma_{F_1}^2 + \sigma_{F_2}^2)], \qquad (7)$$

where σ_D is related to the width of the distribution of the ΔF values; σ_{F_1} and σ_{F_2} are the experimental uncertainties of the structure factor amplitudes. The weight q accounts for the reliability of the structure factor amplitudes, and may be compared with the figure of merit m applied to Fourier maps, that accounts for the reliability of structure factor phases (Read, 1986). The factors m and q thus play parallel roles for the structure factor phases and amplitudes, respectively (Bourgeois, 1999).

The *q*-weighting technique improved difference Fourier maps considerably (Šrajer *et al.*, 1996). However, other sources of systematic errors originating in data collection and processing cannot be corrected this way, for example, errors due to data scaling, incomplete coverage of reciprocal space (§2), mis-assignment of multiples or neglect of energy resolution of Laue spots (§7.1).

5. Applications of Laue diffraction to structural biology

As discussed above, the obvious advantage of the Laue technique is the speed of data collection that may be achieved while maintaining an adequate signal-to-noise ratio, and the small number of exposures necessary to collect complete data sets. This advantage is particularly pronounced when crystals exhibit high symmetry (Clifton *et al.*, 1991). Therefore, Laue diffraction is used when rapid data collection is necessary, under a variety of different circumstances. First, the crystal specimen may not be amenable to flash-freezing (as is frequently the case for virus crystals). Second, the structure at room temperature is desired, but the lifetime of the crystal conditions is too short for conventional monochromatic data collection. Third, although the desired structural state can be established by continuous excitation *via* some physical means, damaging side effects occur. Fourth, the desired structure may be a transient intermediate that cannot be cleanly and uniquely accumulated by physical or chemical trapping; snapshots with high time resolution following reaction initiation in the crystal need to be taken near the chosen time points when the target species reaches a high concentration. Fifth, the concentration of the desired transient intermediate may never reach a high level during the entire time course of the reaction; this species is not detectable at any individual time point, regardless of the time resolution. However, if snapshots with high time resolution are taken at a series of time points, the transient species might be detectable through joint analysis of the time points, by advanced computational means.

The Laue method is almost always linked to data collection at ambient temperatures, either because it is being used for time-resolved experiments under near-physiological conditions, or because it is being used for specimens that are refractory to cryocooling. The fundamental reason is that cryocooling protocols both freeze out the molecular motion and almost always significantly perturb the crystal structure by introducing anisotropic mosaicity. This leads to the conclusion that the Laue

method is best suited for the visualization of intermediate states that cannot be cleanly trapped by cryocooling.

5.1. Design of time-resolved crystallographic studies

In a broad sense, a time-resolved crystallographic experiment can be classified into single- and multi-turnover categories. A single-turnover experiment is an experiment in which one or more exposures are collected during an efficiently triggered single-turnover event or reaction cycle in the crystal, while in a multi-turnover experiment an exposure is taken after the accumulation of a steady-state complex (Moffat, 1989, 1997; Stoddard, 1996a; Stoddard, 1998). In essence, the intrinsic free-energy profile of the reaction is exploited.

One faces several choices of experimental strategy for generation and detection of reaction intermediates in the crystal when designing a time-resolved experiment. Should trapping protocols be applied (Moffat & Henderson, 1995; Stoddard, 1996a)? Is the goal to quench the progression of the reaction past its normal rate-limited step, or alternatively to alter the free-energy profile of the reaction to favour the accumulation of an otherwise short-lived transient intermediate? If no trapping, should one conduct a single-turnover experiment or a multi-turnover steady-state experiment in order to accumulate the transient species being studied? If a single-turnover experiment is chosen, what method of reaction initiation should be used? What method of data collection should be used? In particular, should data collection be conducted using a multi-bunch polychromatic X-ray source (appropriate for microsecond to millisecond time resolution), or a pulse from a single-bunch source (which allows sub-nanosecond time resolution)? Generally, this decision is dictated by the lifetime of intermediate and/or the lifetime of the desired crystal under the experimental conditions.

5.1.1. *Single-turnover experiments.* In a single-turnover experiment a catalytic cycle is triggered *via* a chemical or photochemical event, such that the rate-limited intermediate accumulates and decays in response to the ratio of kinetic rates leading to its formation and decay. The magnitude of the triggering rate k_{start} relative to k_{cat} directly dictates the degree of synchronization of the initial turnover cycle and the homogeneity of the rate-limited complex in the crystal. The faster the turnover and the shorter the half-life of this intermediate, the faster must be the triggering rate for the experiment. The value of k_{start} is equivalent to the slowest event between the initial triggering event and the formation of the productive Michaelis complex, and thus may be as fast as a photolytic event $(10^5 – 10^7 \text{ s}^{-1})$ or as slow as a hindered binding event in the crystal after photolysis (10^2 s^{-1}; Schlichting & Goody, 1997).

5.1.2. *Multi-turnover reactions in crystals and intermediate accumulation.* If the overall turnover rate is sufficiently low, it is possible to drive accumulation of a high-occupancy rate-limited complex throughout the crystal in a steady-state multi-turnover experiment using diffusion to continuously saturate the crystal lattice with a high substrate concentration (Bolduc *et al.*, 1995; Stoddard & Farber, 1995). The key to these experiments is whether diffusion is fast enough to keep up with turnover in the crystal. If so, a monochromatic experiment could in principle be performed to determine the structure of the rate-limited complex. However, under continuous turnover conditions the short lifetime of the crystalline specimen often requires the use of fast Laue diffraction to collect complete data sets over a short period of time.

For such experiments the investigator must be able to provide data indicating that steady-state turnover occurs throughout the crystal (rather than only at the surface of the crystal), and that the resulting experimental electron-density difference maps represent a predominant identifiable species. Full characterization of the crystalline system undergoing turnover may be accomplished by a variety of techniques. These include, first, measurement of the rate of diffusion in the crystal, including an analysis of agreement with established theory and known diffusion rates in solution, which should lead to a well characterized reproducible time period for steady-state formation and saturation of the active sites through the crystal; second, verification that the entire population of enzyme catalysts is involved in steady-state turnover, usually through the measured rate of product formation from the crystal specimen, as well as by direct measurement of spectroscopic absorbance signals in the crystal as an intermediate accumulates; third, the overall turnover rate per active site (expressed in units of s^{-1}) in the crystal relative to solution, and fourth, the effect of the crystal lattice on binding constants, substrate on-rates and individual catalytic steps.

5.1.3. *Decay from a steady state.* A steady state can be established by continuous excitation, a multi-turnover process (§5.1.2) (Stoddard & Farber, 1995; Genick *et al.*, 1997), but the desired intermediate structure may not reach a high concentration at the steady state. Instead, the intermediate may reach a much higher concentration during the decay from the steady state, which can be triggered by cancellation of the excitation. This decay is essentially a single-turnover process (§5.1.1). No example of this combination of single- and multi-turnover experiments has been reported.

5.2. Reaction initiation

In a single crystal of sufficient size for data collection, reaction initiation must be accomplished uniformly and rapidly without damaging the crystal. In principle, one of the following techniques may be used to initiate the reaction in a crystal. First, the concentration of a substrate may be increased by diffusion into the crystal. Second, rapid release of a substrate or co-factor precursor, covalently modified with a photo-releasable blocking group, may be achieved by flashphotolysis. The most rapid reaction initiation (femtoseconds to microseconds) is accomplished by applying a short laser pulse to systems that are naturally photosensitive. Third, the free-energy profile of the system

may be altered by rapidly altering the temperature or pressure. For most experiments where either the initiation step or the subsequent reaction is irreversible, the experiment is reduced to a one-time procedure. In contrast, systems in which the chemical (and physical) changes are fully reversible, such as photoreaction centres, may be repeatedly 'pumped' by the excitation source to allow multiple X-ray exposures.

The simplest method of reaction initiation, diffusion of reactant into the crystal (the first option above), was first described in classic experiments by Wyckoff & Richards (1967), who concluded that diffusion is far too slow for the triggering of anything but exceptionally slow reactions. Subsequent experiments with diffusion and turnover of substrates in enzyme crystals indicated that crystals can be saturated in a minimum of approximately 15 s (specific volume $V_M = 3.5\ \text{Å}^3\,\text{Da}^{-1}$) to well over 100 s ($V_M = 1.8\ \text{Å}^3\,\text{Da}^{-1}$; Stoddard & Farber, 1995). This would indicate that, for a protein crystal of approximately 200 µm in average dimension, synchronization of reaction initiation could be achieved only for systems with k_{cat} less than $10^{-3}\,\text{s}^{-1}$ (half-time of over 10 min). Clearly this is prohibitive for single-turnover time-resolved experiments, but continuous diffusion of high substrate concentrations can drive steady-state accumulation of intermediates formed by enzymes turning over at $0.1\,\text{s}^{-1}$ or slower (Stoddard & Farber, 1995). As derived by Makinen & Fink (1977), a critical thickness l_c can be estimated for most enzyme crystals, such that a steady state can be achieved in the crystal without interference from rate-limiting diffusion processes by using crystals whose smallest dimension do not exceed l_c. This dimension depends on the maximal turnover rate k_{cat} in solution under optimal conditions, the solvent content and solvent channel dimensions in the crystal lattice, and the accessibility of the active sites in the crystal (Makinen & Fink, 1977; Stoddard & Farber, 1995).

The more commonly used method for reaction initiation is the photoactivation of a stable precursor (the second option above; Schlichting & Goody, 1997). This method has included the liberation of a cinnamic acid ester from an active-site catalytic serine residue (Stoddard et al., 1990a), the photorelease of caged substrates including GTP (Schlichting et al., 1989), isocitrate (Brubaker et al., 1996), $NADP^+$ (Cohen et al., 1997) and phosphate (Duke et al., 1994). Well characterized compounds also exist for the photorelease of any caged nucleotide, caged divalent cations (especially magnesium and calcium), caged protons, and caged neurotransmitters (Corrie et al., 1992; Schlichting & Goody, 1997). The most common photoreactive caging groups are nitrobenzyl esters, which may be attached to many different nucleophilic groups, and DM-nitrophen. However, reaction initiation by these caged products typically takes much longer than the laser pulse duration, since it is governed by the release of the caged products via dark reactions, that occur on time scales of microseconds and longer (Peng & Goeldner, 1996; Schlichting & Goody, 1997; Peng et al., 1998) and, in some cases, by local diffusion of the released products to the active sites.

There are a number of parameters that dictate whether flash photolysis can be used to uniformly drive a reaction cycle in a protein crystal (Moffat, 1989; Stoddard, 1996b; Schlichting & Goody, 1997). First, pulsed lasers used for photoinitiation need to be tunable in wavelength to enable selection of a wavelength where the optical density of the crystal is suitably low (0.1), to avoid production of concentration and thermal gradients by photolysis. These gradients frequently introduce crystalline disorder. Transient disorder is often substantially larger than the initial crystal disorder (mosaicity) and may be sufficient to compromise the experiment.

Second, the pulse energy needs to be of the order of 10–100 µJ just to match the number of photons to the number of molecules (10^{13}–10^{14}) in typical-size protein crystals. However, an even higher energy is needed to account for the fact that not all photons are absorbed and, even if absorbed, not all will induce the desired structural reaction if the quantum yield is less than unity. Pulse energies of 10–100 µJ in the wavelength range 400–650 nm with very short laser pulses (100 fs) became available (even commercially) with the development of chirped pulse amplification regenerative amplifiers (Strickland & Mourou, 1985). These very short high-energy pulses have, however, a high potential for crystal damage by the non-linear and dielectric breakdown effects present even in transparent media (Du et al., 1994). A careful investigation is needed to establish the permitted energy levels. Laser systems (nanosecond and femtosecond pulses) that have been implemented at the ID09 beamline at the ESRF and synchronized with the X-ray pulses are described by Bourgeois et al. (1996) and Wulff et al. (1997).

Third, thin crystals (plates or rods) allow quicker diffusion of a substrate and lower optical density, thus more uniform penetration of light relative to thicker crystals, but at the expense of a reduced diffraction volume. Bigger crystals obviously diffract more strongly and therefore improve the quality of the overall data processing by minimizing systematic errors, but are harder to stimulate and monitor optically (Ng et al., 1995). The excited population in a larger crystal may consist of a smaller fraction of the total population, which therefore yields a lower occupancy for the excited structure.

Fourth, the quantum yield (successful photoconversion events per photon absorbed) must be sufficiently high to allow stoichiometric reaction initiation, when a total input power and exposure is used that does not damage the crystal or excessively heat the sample. As a rule of thumb, this corresponds to a quantum yield of 0.4 or greater, although lower values are tolerable if the specimen tolerates a correspondingly greater total flux of excitatory photons.

Fifth, the total heating of the sample can be calculated by estimating the total absorbed laser/flash lamp pulse energy and converting this value to heat; this value can also be

Table 1
Static Laue crystallographic studies.

Protein	Exposure	Experiment	Reference
Ca^{2+} binding protein	30 s	Test photograph	Moffat *et al.* (1984)
Pea lectin	45 s	Test photograph and integration	Helliwell (1984)
Gramicidin A	50 s	Diffraction from small crystal	Hedman *et al.* (1985)
Phosphorylase *b*	1 s	2.4 Å difference maps of substrate	Hajdu, Machin *et al.* (1987)
Xylose isomerase	1 s	Difference Fourier maps of Eu sites	Farber *et al.* (1988)
Insulin	3 s	Change in Zn binding observed	Reynolds *et al.* (1988)
Hen lysozyme	120 ps	Single-bunch Laue diffraction	Szebenyi *et al.* (1988, 1992)
γ-Chymotrypsin	1 s	Peptide observed in active site	Almo (1990)
Turkey lysozyme	1 s	Molecular replacement	Howell *et al.* (1992)
Carbonic anhydrase	3 to 20 s	Complex with bisulfite ion	Lindahl *et al.* (1992)
CO-myoglobin	10 s	Ligand binding	Cameron *et al.* (1993)
Concanavalin A	10 s	Rapid data collection	Cassetta *et al.* (1993)
Hen lysozyme	1 ms	Test new data-processing software	Ren & Moffat (1995*a,b*)
α-Haemolysin	8 ms/12 ms	Test new data-processing software	Ren & Moffat (1995*a,b*)
Cutinase	450 ps	Test single-bunch Laue diffraction	Bourgeois *et al.* (1997)
Restrictocin	0.5 ms/10 ms	1.7 Å resolution refinement	Yang & Moffat (1996), Yang *et al.* (1998)
Acetylcholinesterase	1 ms	Inhibitor binding	Ravelli *et al.* (1998)

measured directly by using microthermocouples in mother liquor samples. As an example, by measuring the total absorbance of CO-myoglobin crystals (0.2 at 635 nm) and knowing the pulse energy (13 mJ), exposure time (7.5 ns), and cross-sectional area of the laser beam (0.44 mm^2) at the crystal, one can calculate that about 0.5–1 mJ of pulse energy was actually absorbed by the crystal (Šrajer *et al.*, 1996). This corresponds to a maximum temperature jump of 10 K, assuming that all the absorbed energy appears as heat.

Sixth, any anisotropic absorbance by the crystal should be accounted for in calculating optical density, heating and reaction yields. Optical anisotropies can be large (Ng *et al.*, 1995).

5.3. *Reaction monitoring*

In order to conduct successful time-resolved experiments *via* both single- and multi-turnover styles, reaction monitoring by a technique other than X-ray diffraction is essential. Changes in optical spectra of the crystals upon reaction initiation have been monitored *in situ* using portable and compact microspectrophotometers (Getzoff *et al.*, 1993; Chen *et al.*, 1994; Hadfield & Hajdu, 1993). These spectroscopic measurements monitor the extent of reaction initiation and reaction progress at the chromophore, and thus provide clues on the time scales in which structural changes can be expected. In addition, they are essential to determine the optimal laser pulse energies sufficient to stimulate the maximum number of molecules in the crystal without causing significant transient or permanent thermal damage.

6. Summary of results in Laue crystallography

Initial quantitative applications of the Laue technique were hampered by lack of thorough understanding of Laue geometry and several computational shortfalls in data processing. In particular, data sets processed from poly-chromatic exposures suffered from a loss of most low-resolution data due to harmonic overlap, and from the need for accurate wavelength normalization (Hajdu *et al.*, 1991). Recent studies have demonstrated that the former problems have been solved through the development of better data-processing algorithms (Ren & Moffat, 1995*a,b*; Clifton *et al.*, 1997; Moffat, 1997; Yang *et al.*, 1998). In general, Laue diffraction data, when collected properly, offer completeness across all resolution bins that rivals monochromatic data. Additionally, Laue data offer the distinct advantage of naturally having high redundancy (§2), allowing accurate data scaling and averaging.

6.1. *Static Laue diffraction studies*

In 1984 the first polychromatic Laue diffraction patterns from protein crystals were reported, with exposure times under 1 min from the first-generation bending-magnet source, CHESS (Moffat *et al.*, 1984). Early reports indicated that intensities could be extracted for most reflections in the Laue patterns (Helliwell, 1984, 1985). Subsequent experiments produced data sets with merging *R*-factors comparable with monochromatic data sets (Helliwell, Gomez de Anderez *et al.*, 1989; Bartunik *et al.*, 1992; Campbell & Hao, 1993) and indicated that such data could be used to calculate interpretable electron density maps (Hajdu, Machin *et al.*, 1987). Since then a large number of static (non-time-resolved) experiments using polychromatic data collection have been reported (Table 1), which emphasize a number of important developments:

Useful exposure times have been lowered to the sub-nanosecond range (Szebenyi *et al.*, 1988, 1992).

Data have been successfully collected and processed from a variety of crystal specimens, including small and slightly disordered crystals (Hedman *et al.*, 1985) and systems with extremely large unit-cell dimensions and unstable behaviour in the X-ray beam, including virus crystals (Campbell *et al.*, 1990).

Table 2
Time-resolved Laue diffraction experiments.

Protein	Time resolution	Experiment	Reference
Hen lysozyme	64 ms	Temperature jump test	Moffat et al. (1986)
Glycogen phosphorylase	1 s	Bound maltoheptose	Hajdu, Machin et al. (1987)
Hen lysozyme	1 s	Radiation damage test	Moffat (1989)
Glycogen phosphorylase	100 ms	Use of caged phosphate	Duke et al. (1994)
Ras oncogene product	1 s	GTP complex	Schlichting et al. (1990)
γ-Chymotrypsin	5 s	Photolysis of cinnamate/pyrone	Stoddard et al. (1991)
Trypsin	800 ms	Ordered hydrolytic water	Singer et al. (1993)
Cytochrome C peroxidase	1 s	Redox active compound I	Fulop et al. (1994)
Hen lysozyme	10 ms	Temperature jump	Chen (1994)
Isocitrate dehydrogenase	50 ms	ES complex and intermediate	Bolduc et al. (1995)
Isocitrate dehydrogenase	10 ms	Product complex	Stoddard et al. (1998)
Photoactive yellow protein	10 ms	pB-like intermediate	Genick et al. (1997)
Photoactive yellow protein	10 ns	pR-like intermediate	Perman et al. (1998)
CO-myoglobin	10 ns	Photolyzed CO species at 290 K	Šrajer et al. (1996)
CO-myoglobin	~1 hr†	Photolyzed CO species at 20–40 K	Teng et al. (1997)
Hydroxymethylbilane synthase	1.5 ms‡	Mutant enzyme-cofactor complex	Helliwell et al. (1998)

† This is the elapsed data collection time; exposure time of each image is 8 ms.   ‡ Achieved time resolution is longer than the exposure time due to diffusion of cofactor in flow cell.

Substrate, inhibitor and metal binding sites have been identified in difference Fourier maps for protein crystals (Hajdu, Acharya et al., 1987; Hajdu, Machin et al., 1987; Farber et al., 1988; Reynolds et al., 1988; Almo, 1990; Campbell et al., 1990).

More recently, polychromatic neutron Laue diffraction experiments have been reported on lysozyme and concanavalin A (Habash et al., 1997; Niimura et al., 1997). These studies are facilitated by advances in detector technologies and improvements in bandwidth for polychromatic neutron sources. The faster data collection afforded by use of Laue geometry allows the behaviour of the protein, under hydrogen–deuterium exchange conditions or during a change of pH, to be more readily monitored through collection of multiple data sets.

A pair of protein structures have been determined by molecular replacement using data collected by the Laue method. In 1992 the structure of turkey egg-white lysozyme was solved and refined at 2.5 Å resolution (Howell et al., 1992). The following year the structure of the glycosomal glyceraldehyde-3-phosphate dehydrogenase was determined at 3.1 Å resolution, also by molecular replacement (Vellieux et al., 1993). This study was notable for its success despite its low data completeness (37%). Both experiments were made necessary by the lack of flash-cooling methods at the time of data collection, and demonstrate the use of the Laue method for rapid conventional data collection.

High-resolution data collection and refinements of outstanding quality have been reported for Laue data collected on several systems, including lysozyme, α-haemolysin and restrictocin (Ren & Moffat, 1995a,b; Yang & Moffat, 1996; Yang et al., 1998). These studies conclusively demonstrated that data sets can be collected to high completeness, including low-resolution shells, to yield structure factor amplitudes of at least the same quality as monochromatic data sets, and that the resulting models

exhibit all of the behaviours in refinement expected for any well determined structure.

Finally, Laue data have been used in small-molecular structure determination by ab initio direct methods (Gomez de Anderez et al., 1989; Helliwell, Gomez de Anderez et al., 1989). In a recent report that may be a harbinger of things to come for macromolecular crystallography, the structures of three different organic compounds have been solved by direct methods after flash-cooling and Laue data collection (Ravelli et al., 1999). This is the first reported use of these techniques in combination for structure determination, and indicates that the increase in mosaicity that accompanies cryocooling, and the deconvolution of low-resolution terms, do not represent insurmountable problems for data processing and ab initio phase calculations.

6.2. Time-resolved Laue diffraction studies

Detailed time-resolved Laue studies have been published on nine separate systems, as summarized below and in Table 2. These studies range from initial work with model systems, intended primarily for the development of techniques for reaction initiation and data collection and processing, to more recent studies that indicate a progression of time-resolved methods to a more mature state. In particular, these studies highlight the successful collection of complete data sets with high time resolution and the successful use of phototriggering for dynamic studies.

6.2.1. *Glycogen phosphorylase: initial time-resolved Laue studies.* Glycogen phosphorylase (GP) catalyzes the reversible conversion of glycogen polymers to glucose-6-phosphate, and constitutes the entry point to glycolysis. In an initial pair of Laue and monochromatic experiments, the binding of maltoheptose to glycogen phosphorylase b was visualized, using data collected prior to and after substrate presentation (Hajdu et al., 1986; Hajdu, Acharya et al.,

1987, Hajdu, Machin *et al.*, 1987). Laue data sets consisting of three exposures each were taken at different angular settings before, during and after presentation of the ligand. Disordering of the crystal lattice was observed in the data set collected during substrate presentation and binding; the disorder was resolved by the time of the final data-set collection. Difference maps calculated with X-ray amplitudes collected prior to and after substrate binding showed clear density for bound maltoheptose at the glycogen binding site. The quality of the Laue map, calculated at 2.5 Å resolution, was clear and easily interpretable. Interestingly, a similar map calculated using experimentally measured monochromatic intensities found in common with the Laue data set was less interpretable. This could be attributed to two factors: reduced radiation damage and identical conditions for obtaining the native and complex data sets. In the Laue experiment, direct scaled differences from a single crystal were used for map calculations, so no wavelength corrections must be applied.

In a continuation of these experiments, 3,5-dinitrophenylphosphate (DNPP) was used as a caged substrate for single-turnover experiments (Duke *et al.*, 1994). After diffusion of DNPP into the T-state GP crystals at concentration between 30 and 45 m*M*, the caged compound bound at the allosteric activator site but not at the catalytic site. Upon photolysis, the liberated phosphate diffused to the catalytic site from the interstitial spaces in the crystal lattice, a distance of 10–50 Å on average. The extremely low affinity of the enzyme for phosphate ($K_m \simeq 35$ m*M*) indicates a very slow on-rate and the need for very high concentrations of liberated phosphate for turnover.

6.2.2. *Ras p21: use of photo-caged substrate as a trigger for a single-turnover experiment*. The gene products of the ras oncogene pathway are involved in signal transduction pathways similar to those involving G proteins. Hydrolysis of the bound nucleotide to GDP leads to a reduction in the signalling activity of the protein. Structural comparison of the protein bound to GTP and to GDP is therefore of considerable interest to investigators studying oncogenic transformation of, and signalling by, the ras pathway.

Schlichting *et al.* (1989) determined that the Ha-ras oncogene product p21 can be crystallized with a photo-labelled GTP derivative, caged GTP, at its active site. After photolytic removal of the protecting group, hydrolysis of GTP to GDP by p21 ras occurs in the crystal at the same rate as in solution, with a half-life for bound GTP of ∼20 min (Schlichting *et al.*, 1989). The appropriate diastereomer of caged GTP binds in the active site with a dissociation constant of 10^{10} M^{-1}, in the same conformation as uncaged nucleotide. Thus, diffusion and binding events after photolysis do not contribute to the rate of bound-substrate formation. The structure of GTP-bound p21 ras was determined using the Laue method after cleavage of the nitrophenylethyl group, before significant hydrolysis had occurred (Schlichting *et al.*, 1990). A second structure was also determined ∼14 min after photolysis, in order to assess the quality and informational content of

data collected well into hydrolysis. The first difference map collected immediately after photolysis confirmed the presence of bound GTP, with the nucleotide bound to the active site in a manner analogous to previous studies with the non-reactive GPPNP. Three phosphate peaks are clearly discernible in the map. A glycine-rich loop is involved in phosphate binding, with a specific hydrogen bond between the amide H-atom of Gly13 and the *b–g* bridging O atom of GTP. The magnesium ion is coordinated to the nucleotide phosphate groups and to the protein by the functional groups of Ser17 and Thr35. No significant conformational or structural differences were found when the structure was compared with bound GPPNP.

6.2.3. *γ-Chymotrypsin: covalent caging and release of a catalytic side chain and visualization of dissociation and subsequent acylation*. In these studies a separate strategy was examined for its utility in triggering single-turnover events through the crystal: covalent caging of an active-site side-chain of the enzyme with a photoreleasable blocking group. Studies centred on whether Laue diffraction data could be used to visualize, in real time, the dissociation of the photoreactive acyl-enzyme complex, followed by binding of a separate inhibitor compound. These experiments also assessed whether covalent caging of the enzyme itself could be an effective strategy for reaction initiation, and whether such experiments could produce difference Fourier maps that clearly discriminate between related chemical and structural species.

Crystals of γ-chymotrypsin inhibited with the photolytically dissociable group *trans-p*-diethylamino-*o*-hydroxy-*a*-methylcinnamate were irradiated with a 1 ms flash from a high-energy xenon flashlamp in the presence of the mechanism-based inhibitor 3-benzyl-6-chloro-2-pyrone (Stoddard *et al.*, 1990*a,b*, 1991). The ensuing reaction was monitored by collection of sequential single-exposure Laue X-ray diffraction patterns. The experiment was also performed in solution in order to verify the regeneration of catalytic activity and the subsequent inhibition of the enzyme by pyrone after photolysis.

The resulting crystallographic structures showed the presence of covalently bound cinnamate prior to photolysis, the generation of a free enzyme after irradiation of the crystal, and the slow formation of a pyrone-inhibited complex several hours after photolysis. The structure of the free enzyme showed a significant proportion of the active sites in the crystal to contain a naturally occurring non-covalently bound tetrapeptide inhibitor even after cinnamate acylation and photolysis. This state persisted in the presence of high pyrone concentrations for several hours, in excellent agreement with the well characterized slow rate of binding of 6-chloropyrone. Data collected simultaneously with irradiation shows the crystal to be slightly disordered during photolysis, leading to streaked Laue spots. The resulting maps are suggestive of a bicyclic coumarin species produced by photolysis and deacylation; however, the electron density was difficult to model unambiguously by a unique chemical state. Nevertheless,

Laue crystallography was shown to be capable of visualizing time-dependent chemical changes in the active site of an enzyme.

6.2.4. *Trypsin: use of a diffusion-triggered pH jump to determine ordered catalytic solvent structure.* Singer *et al.* (1993) demonstrated that it is possible to alter the kinetic profile of a multistep reaction by carefully choosing a specific substrate species, and that a pH-jump can provide an efficient diffusion-based method for triggering a slow catalytic event throughout the crystal. In this case the serine protease trypsin was acylated at the reactive nucleophilic Ser195 by *p*-guanidinobenzoate (GB). This substrate forms an acyl enzyme intermediate readily but is exceedingly slow to undergo hydrolysis and regenerate free enzyme.

A single crystal of GB-bound trypsin was mounted in a flow cell at pH 5.5, and six separate Laue exposures were taken over a period of 5 s. After raising the pH of the buffer directly in a single jump to 8.5, a second series of exposures was obtained. The data sets were processed and individual structures refined to 1.8 Å resolution. The most dramatic feature of the experimental difference maps and results is the appearance immediately after the pH jump of a water molecule that is in a position to attack the scissile bond. The same solvent molecule appears slightly shifted in a later map calculated from data collected ~90 min after the pH jump. An additional feature of the refined models is a gradual shift of the His57 imidazole group of the catalytic triad away from the hydrolytic water molecule during the time-course of the experiment. The hydrolytic water molecule lies directly above the plane of the ester carboxylic group in position for nucleophilic attack, although there is not a hydrogen bond to His57 and the van der Waals contact with the carbonyl C atom is not short enough for good reactivity. The authors hypothesize that the change in protonation state of His57 upon raising the pH is the cause of stabilization and ordering of the incoming hydrolytic water molecule (Singer *et al.*, 1993).

6.2.5. *Cytochrome c peroxidase: use of diffusion to introduce the substrate directly for single-turnover Laue studies.* Cytochrome *c* peroxidase (CCP) is a soluble haem-containing protein found in the mitochondrial electron transport chain where it probably protects against toxic peroxides. The first step of the catalytic reaction involves the reaction of a peroxide with CCP to perform a double oxidation in which the oxidation state of the haem iron is raised from the ferric to the ferryl state (Fe^{4+}) and the indole ring of Trp191 is oxidized to form a free radical. This intermediate state is called compound I and contains one of the O atoms from the peroxide which is now coordinated to the haem iron. In the next step of the catalytic cycle an electron is transferred from the ferrocytochrome *c* to the radical site of Trp191. In the absence of the electron donor, the compound I state is stable for 30–60 min. The aim of this study (Fulop *et al.*, 1994) was to obtain a structure for the rate-limited doubly oxidized transient intermediate in the reaction of CCP with hydrogen peroxide.

Compound I was produced in crystals of yeast CCP by reacting the crystalline enzyme with hydrogen peroxide in a flow cell. The reaction was monitored by microspectrophotometry and Laue crystallography in separate experiments. An almost complete conversion to compound I was achieved within 2 min of addition of hydrogen peroxide, and the concentration of the intermediate remained at similar levels for an additional half-hour. The structure of the intermediate was determined by Laue diffraction. The refined Laue structure for compound I showed clear structural changes at the peroxide-binding site but no significant changes at the radical site. The geometry of the haem environment in this protein allows structural changes to be extremely small, similar in magnitude to those observed for the Fe^{2+}/Fe^{3+} transition in cytochrome *c*. Coordination of the oxygen to the haem iron causes displacement of the iron towards the peroxide-binding site, and the side-chain of a conserved arginine moves to within hydrogen-bonding distance of the ferryl O atom. The results suggest that these molecules have evolved to transfer electrons with a minimal need for structural adjustment.

6.2.6. *Isocitrate dehydrogenase: use of steady-state and single-turnover protocols to visualize separate discrete intermediates.* Isocitrate dehydrogenase (IDH) catalyzes the oxidative decarboxylation of isocitrate to α-ketoglutarate and carbon dioxide, *via* formation of an oxalosuccinate (OSA) intermediate. IDH exhibits a catalytic mechanism with several rapid steps prior to the rate-limiting dissociation of products. The enzyme is fully reactive in the crystal, and under typical conditions (pH 7.5, 295 K) the enzyme turnover rate (60–70 s^{-1}) corresponds to a half-life for the bound product complex of approximately 10 ms, which can be extended to 40–50 ms by moderately lowering either the temperature to 277 K or the pH to 6.5.

In order to accumulate the initial ES complex and the subsequent OSA intermediate, two separate site-directed mutants were used to impose specific kinetic barriers along the reaction coordinate, which resulted in half-lives for specific intermediate species of the order of tens of seconds. These mutants allowed steady-state accumulation of the rate-limited species in the crystal to be combined with Laue data collection and molecular dynamics simulations to describe the structures of two intermediates: the ES complex prior to hydride transfer, and the OSA intermediate formed prior to decarboxylation (Bolduc *et al.*, 1995; Stoddard *et al.*, 1996). Laue data collection was required because of the short lifetime of crystals in the X-ray beam under continuous turnover conditions. In the initial ES complex the most striking structural features revealed by these studies are substrate-dependent and charge-dependent ordering of the NADP nicotinamide and ribose rings. Subsequent substrate perturbation and cryotrapping methods were employed to further study the structural factors that

contribute to an efficient hydride transfer (Mesecar *et al.*, 1997).

Multi-turnover trapping strategies could not be used to visualize the IDH product complex, because no readily available techniques have been identified that significantly increase the lifetime of that species. No protein mutations are known that specifically reduce the rate of product release. Similarly, the conduct of steady-state reactions in the crystal at lower temperatures requires non-viscous cryobuffers that alter the kinetic mechanism of the reaction (glycerol in particular is a non-competitive inhibitor of the reaction), and further reductions in pH alter the rate-limiting step of the reaction. A strategy was therefore chosen that relied on a single-turnover Laue experiment with wild-type enzyme at 277 K (Stoddard *et al.*, 1998). In order to conduct this experiment, several experimental photocaging strategies were used to synchronize the initiation of single initial turnover cycles in the enzyme crystal, in conjunction with Laue data collection. Photolytic liberation of either caged isocitrate or caged NADP and Laue X-ray data collection was used to visualize the complex, which has a minimum half-life of ~10 ms. The experiment was conducted with three different photo-reactive compounds (Brubaker *et al.*, 1996; Cohen *et al.*, 1997), each possessing a unique mechanism leading to the formation of the ES complex. Photoreaction efficiency and subsequent substrate affinities and binding rates in the crystal are critical parameters for these experiments. The structure suggests that CO_2 dissociation is a rapid event that may help drive product formation, and that small conformational changes may contribute to slow product release.

6.2.7. *Photoactive yellow protein: early photocycle inter-mediates.* The PYP protein acts as a receptor for photo-tactic response in halophilic bacteria. The photocycle of the protein, described in its most simple form, consists of a photon-absorption event by a bound *p*-hydroxycinnamyl chromophore in the *trans* conformation of the ground state *P* to produce an electronically excited *P** state that rapidly converts to the first intermediate (*pR*), followed by a protein rearrangement in the millisecond time range to a second intermediate (*pB*) which in turn reverts to the ground state *P* in the 1 s time range (see Fig. 11). The structures of the ground state of the enzyme and of the longest-lived intermediate (*pB*) were determined by multiple isomorphous replacement and by multi-turnover Laue studies using continuous light-pumping, respectively (Borgstahl *et al.*, 1995; Genick *et al.*, 1997). The structural rearrangement upon complete isomerization to the *cis*-conformation in pB and protein relaxation might represent a mechanism for transient signalling, and involves signifi-cant alteration of the protein electrostatic surface.

More recently, two structures of early intermediates during the photocycle of PYP have been determined by different trapping strategies, using either low temperatures and conventional data collection, which allowed visualiza-tion of an early *P**-like excited state (Genick *et al.*, 1998),

or rapid phototriggering and Laue diffraction at ambient temperatures, which allowed visualization of the high-energy *pR* intermediate (Perman *et al.*, 1998). In both structures, prompt isomerization from *trans* to *cis* had occurred. These structures demonstrate that separate time-resolved strategies can yield high-resolution structures of different closely related species on a photochemical reac-tion pathway, and that it is possible to achieve nanosecond time resolution with rapid diffraction techniques.

6.2.8. *Myoglobin: ligand dissociation and trajectory.* A series of experiments on the carbon monoxide complex of myoglobin (MbCO) have visualized the structural processes involved in ligand photodissociation. The experiments have been conducted at cryogenic tempera-ture (Schlichting *et al.*, 1994; Teng *et al.*, 1994, 1997; Hart-mann *et al.*, 1996) and at room temperature (Šrajer *et al.*, 1996), using both monochromatic (Teng *et al.*, 1994; Schlichting *et al.*, 1994; Hartmann *et al.*, 1996) and Laue (Teng *et al.*, 1997; Šrajer *et al.*, 1996) techniques. The initial monochromatic experiments (Teng *et al.*, 1994; Schlichting *et al.*, 1994) conducted at cryogenic temperatures (20–40 K) disagreed quantitatively about the location of the photo-dissociated ligand and the magnitude of the iron displace-ment from the heme plane. The main difference in the experiments was the photolysis protocol used. The photo-dissociated CO was detected farther from its bound loca-tion when the crystals were illuminated continuously during the X-ray data collection (as in Schlichting *et al.*, 1994). In another experiment at 36 K that also employed continuous illumination (Hartmann *et al.*, 1996), an extended CO electron density is observed that spans both CO locations previously observed but the closer location is attributed to the incomplete ligand photolysis. The use of the Laue technique (Teng *et al.*, 1997) allowed reduction of the total elapsed time for the data collection and therefore the collection of several data sets under continuous illu-mination. The results show that after dissociation the CO molecule migrates from an initial location ~1 Å from the binding site to a more distant position ~2.5 Å from the binding site. Taken together, the reported studies reveal different points on the trajectory of the outgoing CO molecule (Teng *et al.*, 1997).

Ligand photodissociation in Mb was also the first reac-tion to be studied by very rapid Laue diffraction techniques in which the X-ray exposure time was only 150 ps, the duration of a single synchrotron X-ray pulse (Bourgeois *et al.*, 1996; Šrajer *et al.*, 1996). A series of data sets collected at different time points, from 4 ns to 1.9 ms after illumi-nation by 7.5 ns laser pulses, clearly revealed ligand photodissociation and rebinding as well as the iron displacement from the heme plane. A potential CO docking site in the heme pocket was identified at ~2 Å from the CO binding site. This location is close to that observed in extended-illumination low-temperature Laue studies (Teng *et al.*, 1997) and in agreement with recent theoretical predictions of the CO probability distribution in the ligand pocket (Vitkup *et al.*, 1997).

6.2.9. *Hydroxymethylbilane synthase: enzyme structure during catalysis*. Hydroxymethylbilane synthase (EC 4.3.1.8, HMBS), also known as porphobilinogen deaminase, is the third enzyme in the biosynthetic pathway of the tetra-pyrroles which include haem, chlorophyll, vitamin B12 and similar pigments. HMBS catalyses the polymerization of four molecules of porphobilinogen to form hydroxy-methylbilane. A dipyrromethane co-factor is present in the HMBS holoenzyme and is covalently attached to the S atom of a cysteine side-chain (Cys242). The co-factor can exist in an oxidized catalytically inactive form and a reduced active form. Four covalent enzyme-substrate intermediate complexes exist in the catalytic pathway, *i.e.* ES1, ES2, ES3, ES4. Previously, the structure of the reduced active form of the selenomethionine-labelled holoenzyme has been solved to 2.4 Å resolution using the MAD method, principally at Daresbury station 9.5 and subsequently also at ESRF BM14 beamline (Hädener *et al.*, 1998). Time-resolved Laue diffraction has been employed at ESRF to study the enzyme structure (Lys59Gln mutant) during catalysis (Helliwell *et al.*, 1997, 1998). The experimental Laue difference maps revealed an elongated difference density peak near the active site, most prominent at 2 h after initiation of substrate diffusion in a flow cell. This peak commenced at the position of ring 2 of the oxidized co-factor (the putative binding site for substrate) and directly above the critical carboxyl side chain of Asp84 which is implicated to be involved in the first ring coupling step (formation of ES1). The density then extended past residues that are known from protein engineering to affect later stages of the catalysis, and into open solvent. There is a missing loop of residues (49–57) in all current HMBS structures undertaken at ambient temperature. The Laue density resides between where that loop is likely to be and the position of the C2 ring in the reduced active cofactor. The time-evolution of this irreversible reaction in the HMBS crystal has thus been established by Laue diffraction, and can guide further Laue and freeze trapping experiments.

7. Ongoing and future developments

We identify several key developments of the Laue crystallography in the near future, which involve the improvements of the technique and its wider applications.

7.1. Crystal with finite mosaic spread

The Laue method exhibits an enhanced sensitivity to crystal mosaicity, and it is necessary to extend Laue analysis strategies to consider biological crystals with appreciable mosaic spread. Although several approaches that deal with elongated Laue diffraction spots from mosaic crystals have been recently developed (§4.3.2), a full treatment of Laue diffraction from anisotropically mosaic crystals is still needed. We demonstrate here the necessity of such a treatment, and leave results for a future report (Z. Ren, unpublished results)

7.1.1. *Elongated spot*. A feature of Laue patterns is that Laue spots are elongated along the radial direction, caused by the mosaic spread of crystal. Consider an isotropic mosaic model, *i.e.* the macroscopic crystal consists of microscopic crystals whose orientation forms a Gaussian distribution around a mean. Every reciprocal lattice point becomes a spherical cap of radius d^* and centred at the origin of reciprocal space O (Fig. 8). Let δ be the mosaic spread in radians. The diffraction ray then consists of a bundle of rays with a range of Bragg angles $\Delta\theta = \delta$, and a range of azimuthal angles

$$\Delta\varphi = \delta/\cos\theta, \qquad (8)$$

where θ is the average Bragg angle. The angular range of the ray bundle normal to $\Delta\theta$ is

$$\Delta\omega = 2\delta\sin\theta. \qquad (9)$$

The ratio of $2\Delta\theta$ and $\Delta\omega$ is an elongation factor

$$e_m = 2\Delta\theta/\Delta\omega = 1/\sin\theta. \qquad (10)$$

Consider a flat detector normal to the X-ray beam. The oblique angle at which each diffraction ray falls on the detector is also along the radial direction. This further elongates all spots by a factor of $1/\cos 2\theta$. Therefore, a Laue spot is elongated by factor e_n in the radial direction:
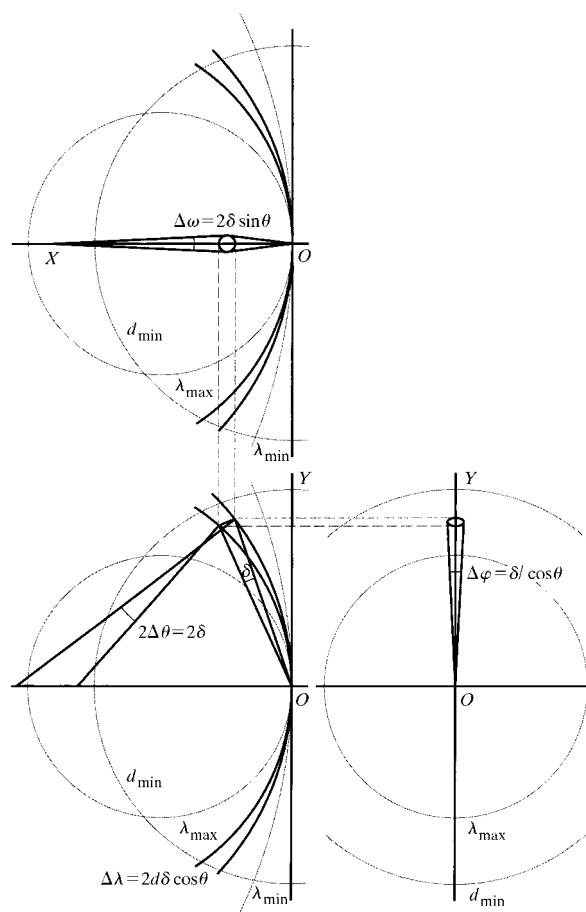

Figure 8
Ewald construction of Laue geometry to show reciprocal lattice 'cap' from finite mosaic spread.

$$e_n = 1/\sin\theta\cos 2\theta. \tag{11}$$

The shape of an experimental Laue spot on the detector arises from four effects: crystal morphology, its mosaicity, X-ray beam convergence or divergence, and oblique angle between the diffraction ray and detector surface. If crystal morphology is also taken into account, and beam convergence is ignored for the moment, the elongation factor becomes

$$e_c = (2\delta M/\cos 2\theta + x)/(2\delta M \sin\theta + x\cos 2\theta), \tag{12}$$

where M is the crystal-to-detector distance and x is the crystal linear dimension.

Thus, the elongation factor is a function of crystal mosaic spread only when crystal morphology is considered. It can be shown that $e_c \leq e_n$; *i.e.* the elongation factor does not diverge indefinitely, as might have been thought previously. The upper limit e_n is independent of crystal mosaic spread δ. Of course, the size of Laue spots is always proportional to the mosaic spread δ. Fig. 9 shows the elongation factors e_c as a function of δ and θ at a crystal-to-detector distance of 100 mm and a crystal dimension of 200 µm.

At a low mosaic spread of 0.1° for example, the spot radial dimension caused by mosaicity is about 370 µm, which is comparable with a typical crystal dimension. All spots are slightly distorted images of the crystal morphology, and no significant elongation is expected. If the mosaic spread is increased to 0.5°, the spot radial and azimuthal dimensions caused by mosaicity are then 2.0 and 0.32 mm, respectively, at a Bragg angle of 10°. This elongation factor of 6.2 is then significantly reduced to ~3.7 by convolution with crystal morphology. If the mosaic spread is further increased to the large value of 2° for example, the spot dimensions 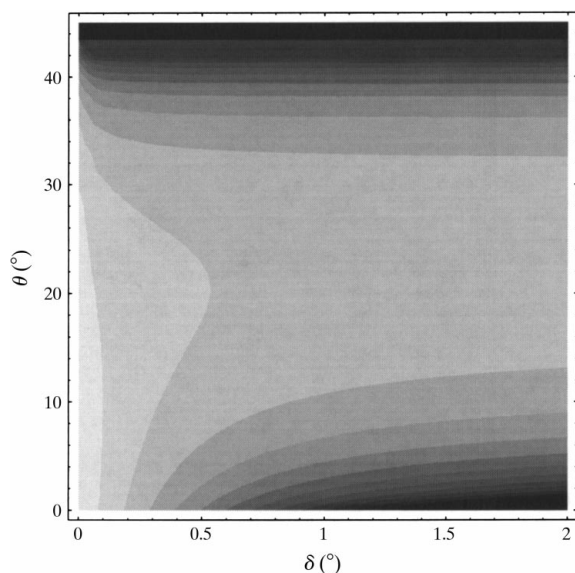will be 7.9 × 1.3 mm for an infinitely small crystal, and 8.1 × 1.5 mm for a 200 µm crystal. The elongation factor of 6.1 is reduced to 5.4.

7.1.2. *Energy resolution of a Laue spot and partial Laue spots.* An unfamiliar aspect implied in equations (11), (12) and Fig. 9 is that the elongation factors of Laue spots increase dramatically at low Bragg angles, even when the crystal is only slightly mosaic. This appears to disagree with the experimental Laue images. Are the elongation factors given by equations (11) and (12) wrong, or are there other factors unaccounted for?

It can be shown (Z. Ren, unpublished results) that the wavelength range $\Delta\lambda$ that stimulates the reciprocal lattice 'cap' with mosaic spread of δ is

$$\Delta\lambda = 2d\delta\cos\theta, \tag{13}$$
$$= \lambda\delta\cot\theta, \tag{14}$$
$$= \delta(4d^2 - \lambda^2)^{1/2}, \tag{15}$$

and

$$\Delta E = -12398\Delta\lambda/\lambda^2, \tag{16}$$

where d is the resolution of the reciprocal cap, and θ and λ are its mean Bragg angle and wavelength, respectively. ΔE is the corresponding energy range in eV, the energy spread of a Laue spot. Fig. 10 shows various surfaces that are derived from equations (13)–(16).

Let the resolution d be 10 Å, the average wavelength λ be 1 Å, and the mosaic spread δ has a moderate value of 0.5°. $\Delta\lambda$ and ΔE are 0.17 Å and 2.2 keV, respectively! Even at a resolution as high as 1 Å, $\Delta\lambda$ and ΔE are significant, 0.015 Å and 190 eV, respectively. The energy spread across a Laue spot from mosaic crystals is much larger than previously thought and is particularly evident at low resolution.

Current Laue data-processing software has not yet accounted for the large energy spread across a Laue spot. This lack is apparently not fatal, as suggested by the numerous successful results summarized in §6. However, the consequences of the large energy spread of a Laue spot are as follows. First, there are an appreciable number of 'partial' Laue spots, in which some energies in the energy spread ΔE lie outside the incident energy range. Second, the spot profile for partial spots may need to be distinguished from other complete spots. Third, there is a potentially important impact on wavelength normalization: it is an over-simplification to assign a single energy or wavelength for each spot. Fourth, harmonic reflections have harmonic $\Delta\lambda$ as well [equation (13)], and complete harmonic deconvolution should account for the effect of energy resolution. Fifth, and most important, mosaicity of the crystal, including anisotropic mosaicity, is the foundation of the above data-processing procedures and should be carefully studied. Laue data quality ought to be further improved if data-processing software are extended to include a correct treatment of energy spread across Laue spots.

Figure 9
Elongation factor e_c [equation (16)] as a function of crystal mosaic spread δ and Bragg angle θ. Darker grey levels indicate larger values of e_c.

To answer the question posed at the beginning of this section, reflections at low Bragg angles are more likely to be partial. Elongation factors of partial spots are smaller than those given by equations (10)–(12). It can be shown that no data at resolution lower than d_p can be recorded as full reflections, where

$$d_p = (\lambda_{max} - \lambda_{min})/2\delta. \qquad (17)$$

For example, if we assume a wide wavelength range of 1 Å and a moderate mosaic spread of 0.5°, d_p is then 57 Å. The single-line undulator U20 at the beamline ID09 of ESRF has a narrow wavelength range of 0.17 Å. The resolution d_p corresponding to the same mosaic spread of 0.5° is then 9.7 Å.

7.1.3. *Laue rotation geometry.* The large energy spread of Laue spots and the presence of partial Laue spots introduce a further challenge to Laue data processing. Nevertheless,

they indicate a new approach to complete data acquisition at very low resolution, by Laue rotation geometry.

At very low resolution and therefore very low Bragg angle, using a fine angular spacing $\Delta\varphi$ during data collection to fill in the low-resolution hole (§2) is not realistic. If, however, the crystal is rotated in a beam of suitably attenuated intensity, a Laue rotation photograph at low Bragg angle will not show elongated spots, even for mosaic crystals. Laue spots are in any case partial at very low resolution d_p [equation (17)] and very low Bragg angle, throughout the rotation. Remarkably, intensities recorded this way require no wavelength normalization, since every reciprocal lattice point/cap traverses the same full spectrum, at a constant angular velocity, the same number of times. Monochromatic rotation geometry (Weisgerber & Helliwell, 1993) offers no advantages over Laue rotation geometry at very low resolution, since a Laue rotation
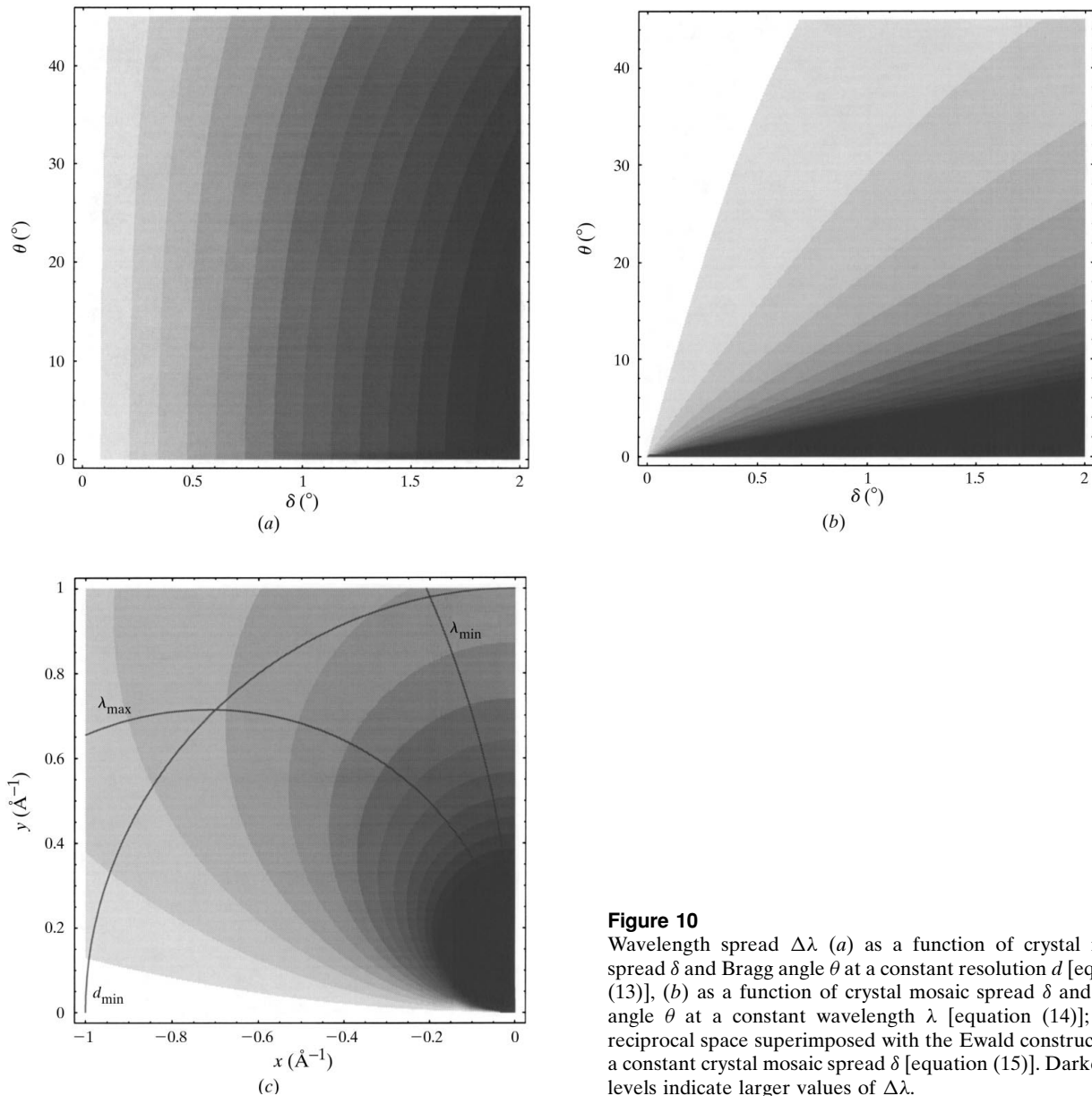

(a)

(b)

(c)

Figure 10
Wavelength spread $\Delta\lambda$ (*a*) as a function of crystal mosaic spread δ and Bragg angle θ at a constant resolution d [equation (13)], (*b*) as a function of crystal mosaic spread δ and Bragg angle θ at a constant wavelength λ [equation (14)]; (*c*) in reciprocal space superimposed with the Ewald construction at a constant crystal mosaic spread δ [equation (15)]. Darker grey levels indicate larger values of $\Delta\lambda$.

image will not show elongated spots due to crystal motion or to crystal mosaicity. Instead, the Laue rotation geometry permits a much larger range of time resolution than monochromatic geometry. Of course, this approach is not suitable for ultrafast time-resolved experiments, since no crystal motion is then possible. However, it might be the right choice for static experiments and slower time-resolved experiments.

7.2. Non-Bragg diffuse scattering

A full understanding of the relationship between the crystal structure and its diffraction pattern requires an explanation of the diffuse scattering as well as the Bragg features. The diffuse features are derived from those parts of the structure which do not obey the symmetry of the crystal, but which may account for a significant fraction of the molecular mass. This fraction may vary during the time course of a reaction: for example, a mobile loop may become more mobile and uncorrelated in conformation from one unit cell to another or, conversely, become ordered through the whole lattice and thereby reduce the fraction of the diffraction pattern that is diffuse. A reasonable prediction of which parts of the structure are more mobile is available from protein structure atomic displacement parameters (ADPs), now available as anisotropic data. In comparison with molecular dynamics trajectories, the excursion of atoms exceeds the ADP values. This indicates that either the molecular dynamics calculations are wrong or that the conformation of molecules in the crystal lattice simply accounts for less than 100% of the accessible conformational space of the protein.
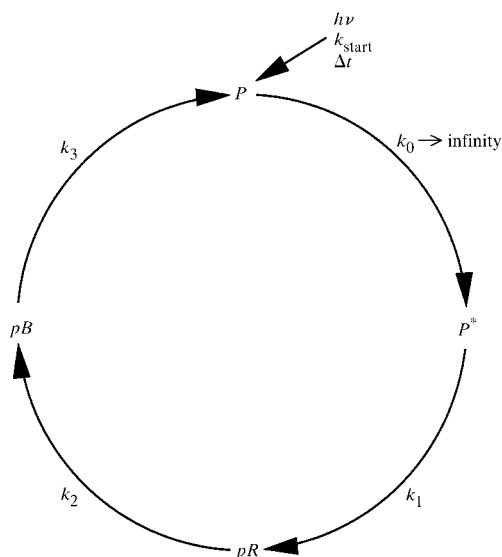

Figure 11
A simplified PYP photocycle with rate constants k_0, k_1, k_2 and k_3. k_0 is the rate determined by the photochemical reaction itself, where we assume that k_0 is approaching infinity. k_{start} is the reaction initiation rate determined by experimental factors such as laser power, quantum yield and optical density of the crystal. The pulse length of reaction initiation is Δt.

Table 3
Rate constants of the simulation in Figs. 12 and 13.

Figure	Δt	k_{start} (s^{-1})	k_0 (s^{-1})	k_1 (s^{-1})	k_2 (s^{-1})	k_3 (s^{-1})
12(a)	0	∞	∞	10^6	10^3	1
12(b)	0	∞	∞	1.1×10^3	10^3	0.9×10^3
12(c)	0	∞	∞	0.5×10^3	10^3	1
12(d)	0	∞	∞	10^6	10^3	2×10^3
13(a)	2 ns	10^9	∞	10^6	10^3	1
13(b)	2 μs	10^6	∞	10^6	10^3	1
13(c)	2 ms	10^3	∞	10^6	10^3	1
13(d)	2 s	10	∞	10^6	10^3	1
13(e)	1 min	0.1	∞	10^6	10^3	1

That is, the lattice constrains the structure. The inter-relationship of ultrahigh-resolution protein structures, with anisotropic ADPs, with time-sliced evolving structures and molecular dynamics calculations, correlated with diffuse scattering observations, offers a rich territory to explore in structure determination. Synchrotron radiation plays a vital role in experimental protein crystallography, sometimes as an adjunct to neutron Laue protein crystallography to elucidate H/D exchange, or for better location of water deuterium atoms.

7.3. Deconvolution of reaction intermediates

Results to date, alluded to in §1, are consistent with the view that in time-resolved macromolecular crystallography the molecules in the crystal behave independently and asynchronously. Their populations rise and fall with time and at any instant the crystal may be composed of a structurally heterogeneous collection of molecules. This is exactly analogous to the situation in dilute solution in which the molecules behave truly independently of one another. Only the behaviour of populations of molecules can be ascertained, for example by spectroscopic means. Time-dependent observations of, for example, a Laue diffraction pattern or the optical absorbance, at a fixed wavelength arise from the time-dependent variation of the populations of time-independent structures, or of species with distinct absorption spectra. Each time-independent structure corresponds to a reaction intermediate and populates the floor of a valley in the free energy *versus* reaction coordinate plot. It follows that a complete experimental structural description would be provided by determination of the structures of all reaction intermediates. These are finite in number, distinct and time-independent. How can they be identified?

The experimental problem may be illustrated by considering the simplified version of the photocycle of PYP (§6.2.7) in Fig. 11. The ground state P absorbs a photon and is converted to a short-lived excited state, P^*; P^* decays rapidly to a spectrally distinct red-shifted intermediate denoted pR; pR in turn decays to a blue-shifted intermediate denoted pB; and pB finally reverts to the ground state P. Figs. 12(a)–12(d) illustrate the fractional population of each intermediate as a function of time on a logarithmic scale for a single-turnover experiment (§5.1.1), with

the conditions and rate constants specified in Table 3 and the figure legend. Notice that the crystal contains more than one structure or reaction intermediate at all times, with the exception of certain time windows in Fig. 12(a) [compare with Fig. 4 of Moffat et al. (1992)] when all molecules in the crystal transiently occupy a certain intermediate. Figs. 13(a)–13(e) illustrate the effect of a protracted reaction initiation step k_{start} (§5). The populations in Fig. 12(a) are altered by varying the rate of initiation k_{start} and the pulse length of the initiation Δt (Table 3). A 2 ns initiation with $k_{start} = 10^9 \text{ s}^{-1}$ corresponds to an initiating light pulse from an Nd:YAG pumped dye laser [Fig. 13(a); Bourgeois et al., 1996; Perman et al., 1998]. A 2 µs initiation with $k_{start} = 10^6 \text{ s}^{-1}$ corresponds to a flash-lamp-pumped dye laser [Fig. 13(b)]; the maximum achievable concentration of P^* is much lower. A 2 ms initiation with $k_{start} = 10^3 \text{ s}^{-1}$ corresponds to the time-course of release of a caged compound [Fig. 13(c)]. A 2 s initiation with $k_{start} = 10 \text{ s}^{-1}$ corresponds to illumination by a CW Ar laser [Fig. 13(d); Ng et al., 1995; Genick et al., 1997]; only a trace amount of pR is present even at its peak concentration, and the time at which the peak concentration of pB is

obtained is considerably delayed [1 s in Fig. 13(d) compared with 10 ms in Figs. 13(a)–13(c)]. A 1 min initiation with $k_{start} = 0.1 \text{ s}^{-1}$ corresponds to diffusion of substrate in a flow cell [Fig. 13(e)]; no intermediate can accumulate to a significant peak concentration. That is, there is a failure in initiation for reaction of these rates. The more protracted the reaction initiation, the lower the peak population and the less detectable are the shorter-lived intermediates (§5).

This PYP example illustrates the case in which the overall reaction mechanism (or a good approximation to it) is known: the number of reaction intermediates and the pathways and rate constants by which they are interconverted. In general, this is not the case. It is necessary then to acquire time-resolved crystallographic data, uniformly spaced in the logarithm of time (B. Perman and colleagues, unpublished results). From such data, can the reaction mechanism be objectively deduced? Can the time-independent structures of each intermediate be 'deconvoluted' from the time-dependent data? Some ideas on how to proceed were proposed by Moffat (1989). Analysis could proceed in reciprocal space. Exponential or other func-
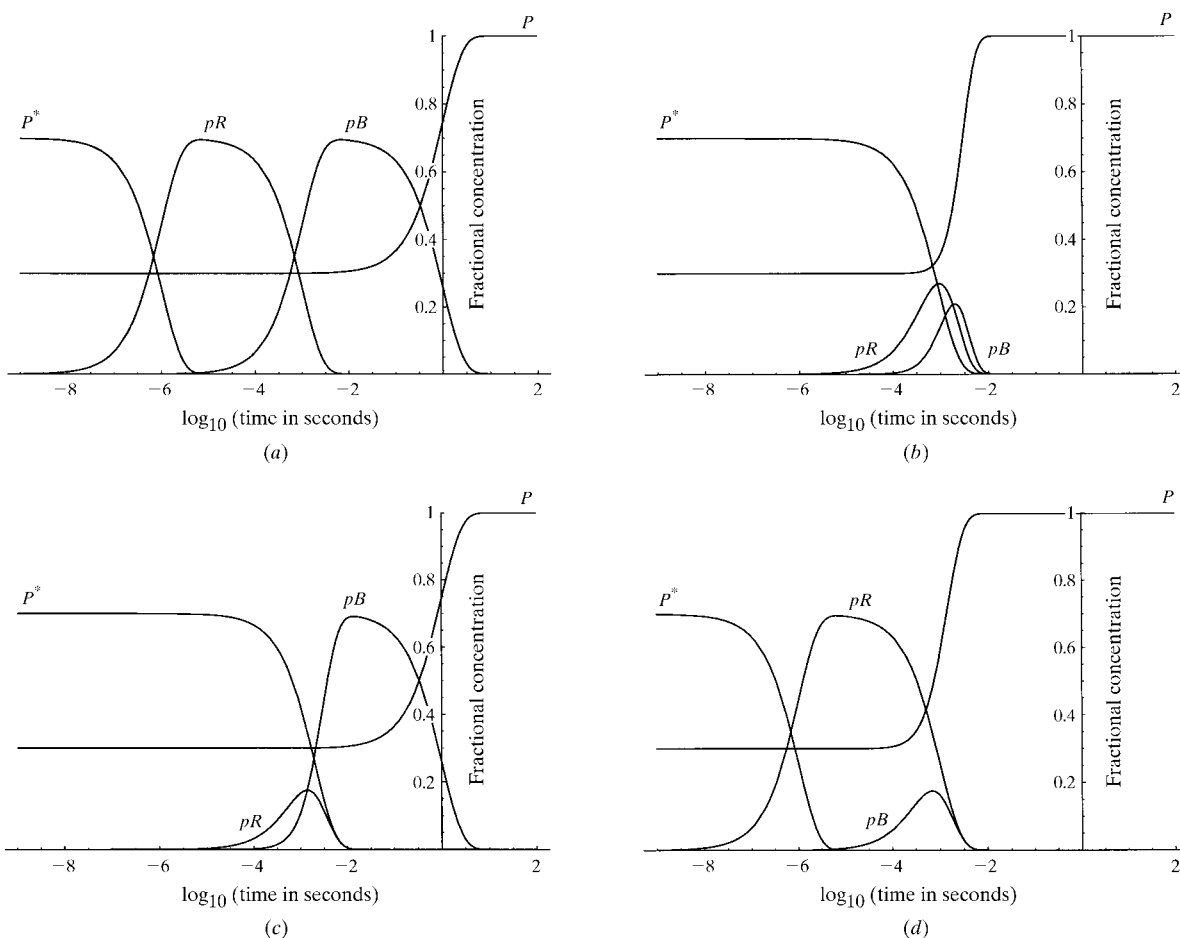

Figure 12

Simulation of the fractional concentrations for the structural species in the PYP photocycle shown in Fig. 11 with different rate constants k_1, k_2 and k_3 in Table 3. We assume the initiation laser pulse follows a δ function, i.e. $\Delta t = 0$, laser power is infinity, and the total laser energy is sufficient to excite 70% of the PYP molecules.

tional fitting to the time-dependent structure amplitudes could be followed by consideration of each of the small number of mechanisms that display the observed number of exponents. Each mechanism could be evaluated in real space through recognition that an authentic structural intermediate must be a single refinable protein structure. Alternatively, analysis could proceed in real space. Singular value decomposition or principal component analysis could extract the maximum number of independent electron density subdistributions, each presumably corresponding to an intermediate, from the time-dependent average electron density distributions. More likely, analysis will proceed *via* a blend of reciprocal and real space approaches. It may ultimately be possible to crystallographically refine all intermediate structures simultaneously, against the complete set of time-dependent observations over 100 or so time points.

7.4. Genomics

The context of monochromatic and Laue time-resolved development is rapid growth in both static and dynamic structure-determination capability, reaching up to the
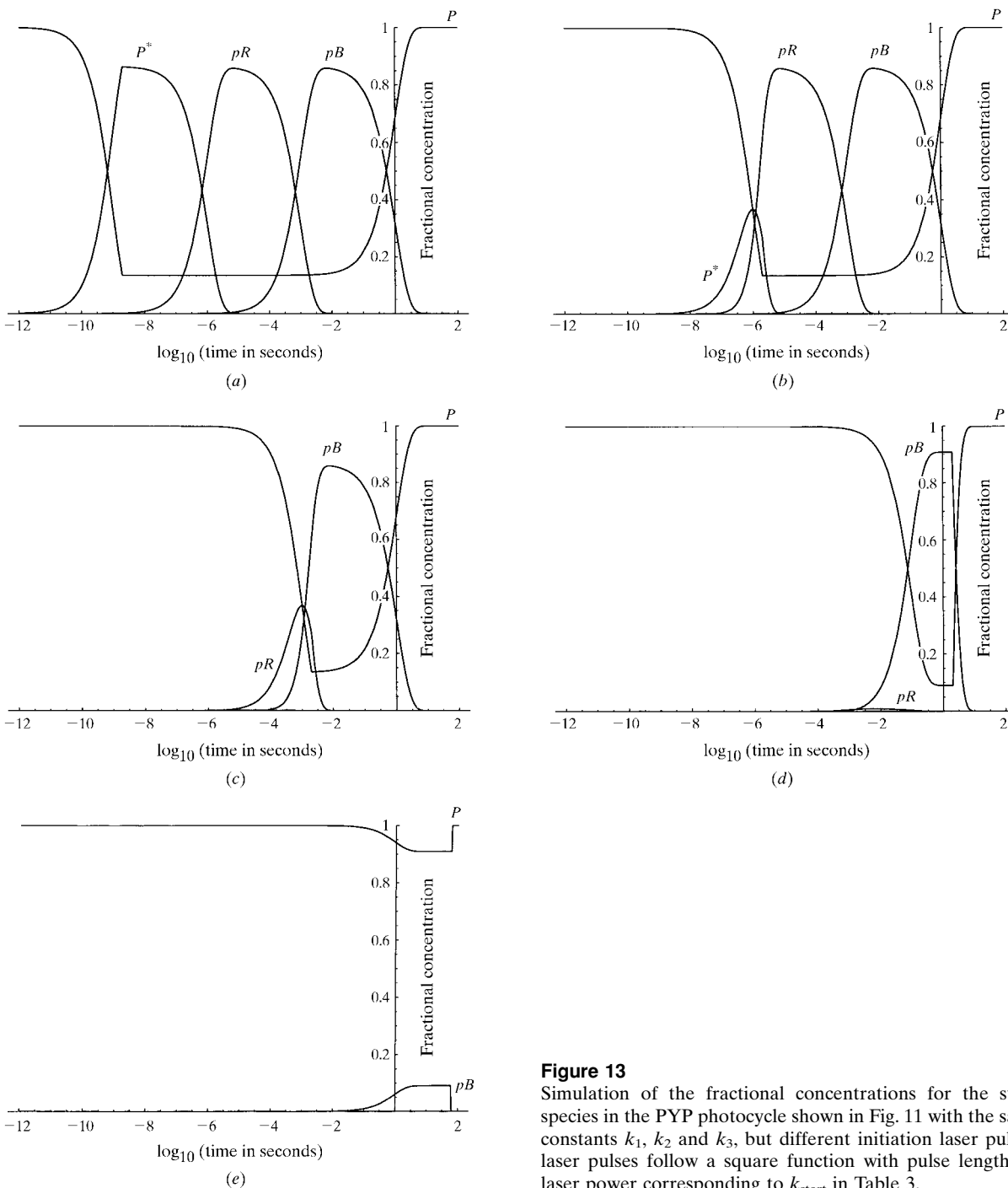

Figure 13
Simulation of the fractional concentrations for the structural species in the PYP photocycle shown in Fig. 11 with the same rate constants k_1, k_2 and k_3, but different initiation laser pulses. The laser pulses follow a square function with pulse length Δt and laser power corresponding to k_{start} in Table 3.

level of whole genomes. There are several aspects to this. The term 'genomics' is concerned with the determination and study of the nucleotide sequences of all the genes in an organism. From these the amino acid sequences are inferred *via* the genetic code; this forms part of what is now known as 'proteomics'. 'Functional genomics' is the term coined for the prediction of the functionally important proteins in a genome, as many are in fact apparently redundant or 'silent'. Prediction of protein folds from amino acid sequences seeks to identify new folds, a further part of proteomics; these proteins as a group obviously may not overlap fully with the functionally important group. Detailed exploration of certain proteins to explore their reactivity or functional dynamics *via* time-resolved crystallography may be regarded as a part of functional genomics, or may warrant coining a further term such as 'dynomics'. It is in this spirit that time-resolved structural analyses seek to reveal in detail workings of a biological macromolecule, and its interactions with other molecules in the organelle or organism in, for example, a lengthy signal transduction pathway, or in a metabolic pathway. Thus the discipline of biochemistry prefers the selected structure determination approach to proteomics: only seek the structure of those proteins we know to be physiologically interesting. Time-resolved Laue crystallography has a close affinity with this view as it concentrates on the inner workings of a few functionally important and possibly representative proteins, rather than marching onwards to the next '*de novo*' protein structure determination.

8. Conclusions

In Laue protein crystallography we are seeking to expand direct experimental approaches to protein structure and function elucidation, and believe that the field of Laue crystallography is coming of age. This is to say the conception of ideas, the formulation of plans, the implementation including the correction of errors and the execution to a variety of both test and actual time-resolved dynamical applications of both reversible and irreversible processes, have been realised. This is not to say that further technical developments are not possible. On the contrary, considerable further developments will come (§7). These developments will push back the frontiers, to include more complicated structural processes, the study of yet faster processes, and identification of transient intermediates with low peak occupancy, over all timescales from picoseconds to kiloseconds. As the results of Laue experiments, published or soon to be published, become more visible in the structural biology and chemistry communities, we confidently predict that the Laue technique will be applied to a wider variety of biological systems, by an expanded circle of investigators. That is, the Laue technique will enter the third mature stage of technique development noted in the *Introduction*.

References

Almo, S. C. (1990). *Biochemistry and Biophysics*, pp. 150. Harvard University, Cambridge, MA, USA.
Arzt, S., Campbell, J. W., Harding, M. M., Hao, Q. & Helliwell, J. R. (1999). *J. Appl. Cryst.* In the press.
Bartunik, H. D., Bartsch, H. H. & Qichen, H. (1992). *Acta Cryst.* A**48**, 180–188.
Bolduc, J. M., Dyer, D. H., Scott, W. G., Singer, P., Sweet, R. M., Koshland, D. E. Jr & Stoddard, B. L. (1995). *Science*, **268**, 1312–1318.
Borgstahl, G. E. O., Williams, D. R. & Getzoff, E. D. (1995). *Biochemistry*, **34**, 6278–6287.
Bourenkov, G. P., Popov, A. N. & Bartunik, H. D. (1996). *Acta Cryst.* A**52**, 797–811.
Bourgeois, D. (1999). *Acta Cryst.* D. Submitted.
Bourgeois, D., Longhi, S., Wulff, M. & Cambillau, C. (1997). *J. Appl. Cryst.* **30**, 153–163.
Bourgeois, D., Nurizzo, D., Kahn, R. & Cambillau, C. (1998). *J. Appl. Cryst.* **31**, 22–35.
Bourgeois, D., Schotte, F. & Wulff, M. (1999). In preparation.
Bourgeois, D., Ursby, T., Wulff, M., Pradervand, C., LeGrand, A., Schildkamp, W., Laboure, S., Šrajer, V., Teng, T.-Y., Roth, M. & Moffat, K. (1996). *J. Synchrotron Rad.* **3**, 65–74.
Bradbrook, G., Deacon, A., Habash, J., Helliwell, J. R., Helliwell, M., Nieh, Y. P., Raftery, J., Snell, E. H., Trapani, S., Thompson, A. W., Campbell, J. W., Allinson, N. M., Moon, K., Ursby, T. & Wulff, M. (1997). *Time-Resolved Diffraction*, edited by J. R. Helliwell & P. M. Rentzepis, pp. 166–186. Oxford University Press.
Brubaker, M. J., Dyer, D. H., Stoddard, B. & Koshland, D. E. Jr (1996). *Biochemistry*, **35**, 2854–2864.
Cameron, A. D., Smerdon, S. J., Wilkinson, A. J., Habash, J., Helliwell, J. R., Li, T. & Olson, J. S. (1993). *Biochemistry*, **32**, 13061–13070.
Campbell, J. W. (1995). *J. Appl. Cryst.* **28**, 228–236.
Campbell, J. W. & Hao, Q. (1993). *Acta Cryst.* A**49**, 889–893.
Campbell, J. W., Clifton, I. J., Greenhough, T. J., Hajdu, J., Harrison, S. C., Liddington, R. C. & Shrive, A. K. (1990). *J. Mol. Biol.* **214**, 627–632.
Campbell, J. W., Habash, J., Helliwell, J. R. & Moffat, K. (1986). *Inf. Q. Protein Cryst.* **18**, 23–31. Warrington: Daresbury Laboratory.
Campbell, J. W., Hao, Q., Harding, M. M., Nguti, N. D. & Wilkinson, C. (1998). *J. Appl. Cryst.* **30**, 496–502.
Carr, P. D., Cruickshank, D. W. J. & Harding, M. M. (1992). *J. Appl. Cryst.* **25**, 294–308.
Carr, P. D., Dodd, I. M. & Harding, M. M. (1993). *J. Appl. Cryst.* **26**, 384–387.
Cassetta, A., Deacon, A., Emmerich, C., Habash, J., Helliwell, J. R., MacSweeney, S., Snell, E., Thompson, A. W. & Weisgerber, S. (1993). *Proc. R. Soc. A*, **442**, 177–192.
Chen, Y. (1994). PhD thesis, Cornell University, USA.
Chen, Y., Šrajer, V., Ng, K., LeGrand, A. & Moffat, K. (1994). *Rev. Sci. Instrum.* **65** 1506–1511.
Clifton, I. J., Duke, E. M. H., Wakatsuki, S. & Ren, Z. (1997). *Methods Enzymol.* **277**, 448–467.
Clifton, I. J., Elder, M. & Hajdu, J. (1991). *J. Appl. Cryst.* **24**, 267–277.
Cohen, B. E., Stoddard, B. L. & Koshland, D. E. Jr (1997). *Biochemistry*, **36**, 9035–9044.
Corrie, J. E. T., Katayama, Y., Reid, G. P., Anson, M. & Trentham, D. R. (1992). *Philos. Trans. R. Soc. London*, A**340**, 233–244.
Cruickshank, D. W. J., Helliwell, J. R. & Moffat, K. (1987). *Acta Cryst.* A**43**, 656–674.
Cruickshank, D. W. J., Helliwell, J. R. & Moffat, K. (1991). *Acta Cryst.* A**47**, 352–373.

Du, D., Liu, X., Korn, G., Squier, J. & Mourou, G. (1994). *Appl. Phys. Lett.* **64**, 3071–3073.

Duke, E. M. H., Wakatsuki, W., Hadfield, A. & Johnson, L. N. (1994). *Protein Sci.* **3**, 1178–1196.

Farber, G. K., Machin, P. A., Almo, S. C., Petsko, G. A. & Hajdu, J. (1988). *Proc. Natl Acad. Sci USA*, **85**, 112–115.

Fisher, A. J., McKinney, B. R., Wery, J. P. & Johnson, J. E. (1992). *Acta Cryst.* B**48**, 515–520.

Fulop, V., Phizackerley, R. P., Soltis, S. M., Clifton, I. J., Wakatsuki, S., Erman, J., Hajdu, J. & Edwards, S. L. (1994). *Structure*, **2**, 201–208.

Genick, U. K., Borgstahl, G. E. O., Ng, K., Ren, Z., Pradervand, C., Burke, P. M., Šrajer, V., Teng, T.-Y., Schildkamp, W., McRee, D. E., Moffat, K. & Getzoff, E. D. (1997). *Science*, **275**, 1471–1475.

Genick, U. K., Soltis, S. M., Kuhn, P., Canestrelli, I. L. & Getzoff, E. D. (1998). *Nature (London)*, **392**, 206–209.

Getzoff, E. D., Jones, K. W., McRee, D., Moffat, K., Ng, K., Rivers, M. L., Schildkamp, W., Singer, P. T., Spanne, P., Sweet, R. M., Teng, T.-Y. & Westbrook, E. M. (1993). *Nucl. Instrum. Methods Phys. Res. B*, **79**, 249–255.

Gomez de Anderez, D., Helliwell, M., Habash, J., Dodson, E. J., Helliwell, J. R., Bailey, P. D. & Gammon, R. E. (1989). *Acta Cryst.* B**45**, 482–488.

Greenhough, T. J. & Shrive, A. K. (1994). *J. Appl. Cryst.* **27**, 111–121.

Habash, J., Raftery, J., Weisgerber, S., Cassetta, A., Lehmann, M. S., Hoghoj, P., Wilkinson, C., Campbell, J. W. & Helliwell, J. R. (1997). *J. Chem. Soc. Faraday Trans.* **93**, 4313–4317.

Hadfield, A. & Hajdu, J. (1993). *J. Appl. Cryst.* **26**, 839–842.

Hädener, A., Matzinger, P. K., Battersby, A. R., McSweeney, S., Thompson, A. W., Hammersley, A. P., Harrop, S. J., Cassetta, A., Deacon, A., Hunter, W. N., Nieh, Y. P., Raftery, J., Hunter, N. & Helliwell, J. R. (1998). *Acta Cryst.* D**55**, 631–643.

Hajdu, J., Acharya, K. R., Stuart, D. I., McLaughlin, P. J., Barford, D., Klein, H. & Johnson, L. N. (1986). *Biochem. Soc. Trans.* **14**, 538–541.

Hajdu, J., Acharya, K. R., Stuart, D. I., McLaughlin, P. J., Barford, D., Klein, H., Oikonomakos, N. G. & Johnson, L. N. (1987). *EMBO J.* **6**, 539–546.

Hajdu, J., Almo, S. C., Farber, G. K., Prater, J. K., Petsko, G. A., Wakatsuki, S., Clifton, I. J. & Fulop, V. (1991). *Crystallographic Computing 5*, edited by D. Moras, A. D. Podjarny & J. C. Thierry, pp. 29–49. Oxford University Press.

Hajdu, J., Machin, P. A., Campbell, J. W., Greenhough, T. J., Clifton, I. J., Zurek, S., Gover, S., Johnson, L. N. & Elder, M. (1987). *Nature (London)*, **329**, 178–181.

Hanley, Q. S., Dunphy, D. R. & Denton, M. B. (1996). *J. Synchrotron Rad.* **3**, 101–111.

Hao, Q., Campbell, J. W., Harding, M. M. & Helliwell, J. R. (1993). *Acta Cryst.* A**49**, 528–531.

Hao, Q., Harding, M. M. & Campbell, J. W. (1995). *J. Appl. Cryst.* **28**, 447–450.

Hartmann, H., Zinser, S., Komninos, P., Schneider, R. T., Nienhaus, G. U. & Parak, F. (1996). *Proc. Natl Acad. Sci. USA*, **93**, 7013–7016.

Hedman, B., Hodgson, K., Helliwell, J. R., Liddington, R. C. & Papiz, M. Z. (1985). *Proc. Natl Acad. Sci. USA*, **82**, 7604–7606.

Helliwell, J. R. (1984). *Rep. Prog. Phys.* **47**, 1403–1497.

Helliwell, J. R. (1985). *J. Mol. Struct.* **130**, 63–91.

Helliwell, J. R. (1991). *Nucl. Instrum. Methods*, A**308**, 260–266.

Helliwell, J. R. (1992). *Macromolecular Crystallography with Synchrotron Radiation.* Cambridge University Press.

Helliwell, J. R. (1997). *Methods Enzymol.* **276**, 203–217.

Helliwell, J. R., Habash, J., Cruickshank, D. W. J., Harding, M. M., Greenhough, T. J., Campbell, J. W., Clifton, I. J., Elder, M., Machin, P. A., Papiz, M. Z. & Zurek, S. (1989). *J. Appl. Cryst.* **22**, 483–497.

Helliwell, J. R., Harrop, S., Habash, J., Magorrian, B. G., Allinson, N. M., Gomez, D., Helliwell, M., Derewenda, Z. & Cruickshank, D. W. J. (1989). *Rev. Sci. Instrum.* **60**, 1531–1536.

Helliwell, J. R., Nieh, Y. P., Cassetta, A., Raftery, J., Haedener, A., Niemann, A. C., Battersby, A. R., Carr, P. D., Wulff, M., Ursby, T., Moy, J. P. & Thompson, A. W. (1997). *Time-Resolved Diffraction*, edited by J. R. Helliwell & P. M. Rentzepis, pp. 187–194. Oxford University Press.

Helliwell, J. R., Nieh, Y. P., Raftery, J., Cassetta, A., Habash, J., Carr, P. D., Ursby, T., Wulff, M., Thompson, A. W., Niemann, A. C. & Hädener, A. (1998). *J. Chem. Soc. Faraday Trans.* **94**, 2615–2622.

Helliwell, M., Gomez de Anderez, D., Habash, J., Helliwell, J. R. & Vernon, J. (1989). *Acta Cryst.* B**45**, 591–596.

Howell, P. L., Almo, S. C., Parsons, M. R., Hajdu, J. & Petsko, G. A. (1992). *Acta Cryst.* B**48**, 200–207.

LeGrand, A. D., Schildkamp, W. & Blank, B. (1989). *Nucl. Instrum. Methods*, A**275**, 442–446.

Lindahl, M., Liljas, A., Habash, J., Harrop, S. & Helliwell, J. R. (1992). *Acta Cryst.* B**48**, 281–285.

Makinen, M. W. & Fink, A. L. (1977). *Ann. Rev. Biophys. Bioeng.* **6**, 301–343.

Mesecar, A. D., Stoddard, B. L. & Koshland, D. E. Jr (1997). *Science*, **277**, 202–206.

Moffat, K. (1989). *Ann. Rev. Biophys. Biophys. Chem.* **18**, 309–332.

Moffat, K. (1997). *Methods Enzymol.* **277**, 433–447.

Moffat, K. (1998a). *Nat. Struct. Biol.* **5**, 641–643.

Moffat, K. (1998b). *Acta Cryst.* A**54**, 833–841.

Moffat, K., Bilderback, D., Schildkamp, W. & Volz, K. (1986). *Nucl. Instrum. Methods Phys. Res. A*, **246**, 627–635.

Moffat, K., Chen, Y., Ng, K., McRee, D. & Getzoff, E. D. (1992). *Philos. Trans. R. Soc. London*, A**340**, 175–190.

Moffat, K. & Henderson, R. (1995). *Curr. Opin. Struct. Biol.* **5**, 656–663.

Moffat, K., Szebenyi, D. & Bilderback, D. (1984). *Science*, **223**, 1423–1425.

Ng, K., Getzoff, E. D. & Moffat, K. (1995). *Biochemistry*, **34**, 879–890.

Niimura, N., Minezaki, Y., Nonaka, T., Castagna, J.-C., Cipriani, F., Hoghoj, P., Lehmann, M. S. & Wilkinson, C. (1997). *Nat. Struct. Biol.* **4**, 909–914.

Peng, L. & Goeldner, M. (1996). *J. Org. Chem.* **61**, 185–191.

Peng, L., Nachon, F., Wirz, J. & Goeldner, M. (1998). *Angew. Chem. Int. Ed.* **37**, 2691–2693.

Perman, B., Šrajer, V., Ren, Z., Teng, T.-Y., Pradervand, C., Ursby, T., Bourgeois, D., Schotte, F., Wulff, M., Kort, R., Hellingwerf, K. & Moffat, K. (1998). *Science*, **279**, 1946–1950.

Ravelli, R. B. G. (1998). PhD thesis, Utrecht University, The Netherlands.

Ravelli, R. B. G., Hezemans, A. M. F., Krabbendam, H. & Kroon, J. (1996). *J. Appl. Cryst.* **29**, 270–278.

Ravelli, R. B. G., Raves, M. L., Ren, Z., Bourgeois, D., Roth, M., Kroon, J., Silman, I. & Sussman, J. (1998). *Acta Cryst.* D**54**, 1359–1366.

Ravelli, R. B. G., Raves, M. L., Scheres, S. H. W., Schouten, A. & Kroon, J. (1999). *J. Synchrotron Rad.* **6**, 19–28.

Read, R. (1986). *Acta Cryst.* A**42**, 140–149.

Ren, Z. & Moffat, K. (1994). *J. Synchrotron Rad.* **1**, 78–82.

Ren, Z. & Moffat, K. (1995a). *J. Appl. Cryst.* **28**, 461–481.

Ren, Z. & Moffat, K. (1995b). *J. Appl. Cryst.* **28**, 482–493.

Ren, Z., Ng, K., Borgstahl, G. E. O., Getzoff, E. D. & Moffat, K. (1996). *J. Appl. Cryst.* **29**, 246–260.

Ren, Z., Sheng, R. & Wright, S. J. (1999). *Int. J. Supercomput. Appl.* Submitted.

Reynolds, C. D., Stowell, B., Joshi, K. K., Harding, M. M., Maginn, S. J. & Dodson, G. G. (1988). *Acta Cryst*, B**44**, 512–515.

Ringe, D., Stoddard, B. L., Bruhnke, J., Koenigs, P. & Porter, N. (1992). *Philos. Trans. R. Soc. London Ser. A*, **340**, 273–284.

Rossmann, M. G. (1979). *J. Appl. Cryst.* **12**, 225–238.

Schlichting, I., Almo, S. C., Rapp, G., Wilson, K., Petratos, K., Lentfer, A., Wittinghofer, A., Kabsch, W., Pai, E. F., Petsko, G. A. & Goody, R. S. (1990). *Nature (London)*, **345**, 309–315.

Schlichting, I., Berendzen, J., Phillips, G. N. Jr & Sweet, R. M. (1994). *Nature (London)*, **371**, 808–812.

Schlichting, I. & Goody, R. S. (1997). *Methods Enzymol.* **277**, 467–490.

Schlichting, I., Rapp, G., John, J., Wittinghofer, A., Pai, E. F. & Goody, R. S. (1989). *Proc. Natl Acad. Sci. USA*, **86**, 7687–7690.

Shrive, A. K., Clifton, I. J., Hajdu, J. & Greenhough, T. J. (1990). *J. Appl. Cryst.* **23**, 169–174.

Singer, P. T., Smalås, A., Carty, R. P., Mangel, W. F. & Sweet, R. M. (1993). *Science*, **259**, 669–673.

Smith Temple, B. R. (1989). PhD thesis, Cornell University, USA.

Šrajer, V., Ren, Z., Moffat, K. *et al.* (1999). In preparation.

Šrajer, V., Teng, T.-Y., Ursby, T., Pradervand, C., Ren, Z., Adachi, S., Schildkamp, W., Bourgeois, D., Wulff, M. & Moffat, K. (1996). *Science*, **274**, 1726–1729.

Stoddard, B. L. (1996a). *Nat. Struct. Biol.* **3**, 907–909.

Stoddard, B. L. (1996b). *Pharmacol. Ther.* **70**, 215–256.

Stoddard, B. L. (1998). *Curr. Opin. Struct. Biol.* **8**, 612–618.

Stoddard, B. L., Bruhnke, J., Koenigs, P., Porter, N., Ringe, D. & Petsko, G. (1990a). *Biochemistry*, **29**, 8042–8051.

Stoddard, B. L., Bruhnke, J., Porter, N., Ringe, D. & Petsko, G. A. (1990b). *Biochemistry*, **29**, 4871–4879.

Stoddard, B. L., Cohen, B. E., Brubaker, M., Mesecar, A. D. & Koshland, D. E. (1998). *Nat. Struct. Biol.* **5**, 891–897.

Stoddard, B. L., Dean, A. & Bash, P. A. (1996). *Nat. Struct. Biol.* **3**, 590–595.

Stoddard, B. L. & Farber, G. K. (1995). *Structure*, **3**, 991–996.

Stoddard, B. L., Koenigs, P., Porter, N., Petratos, K., Petsko, G. A. & Ringe, D. (1991). *Proc. Natl Acad. Sci. USA*, **88**, 5503–5507.

Strickland, D. & Mourou, G. (1985). *Opt. Commun.* **56**, 219–221.

Sweet, R. M., Singer, P. T. & Smalås, A. (1993). *Acta Cryst.* D**49**, 305–307.

Szebenyi, D. M. E., Bilderback, D. H., LeGrand, A., Moffat, K., Schildkamp, W., Smith Temple, B. & Teng, T.-Y. (1988). *Trans. Am. Cryst. Assoc.* **24**, 167–172.

Szebenyi, D. M. E., Bilderback, D. H., LeGrand, A., Moffat, K., Schildkamp, W., Smith Temple, B. & Teng, T.-Y. (1992). *J. Appl. Cryst.* **25**, 414–423.

Teng, T.-Y., Šrajer, V. & Moffat, K. (1994). *Nat. Struct. Biol.* **1**, 701–705.

Teng, T.-Y., Šrajer, V. & Moffat, K. (1997). *Biochemistry*, **36**, 12087–12100.

Terwilliger, T. C. & Berendzen, J. (1995). *Acta Cryst.* D**51**, 609–618.

Terwilliger, T. C. & Berendzen, J. (1996). *Acta Cryst.* D**52**, 743–748.

Ursby, T. & Bourgeois, D. (1997). *Acta Cryst.* A**53**, 564–575.

Vellieux, F. M. D., Hajdu, J., Verlinde, C. L. M. J., Groendijk, H., Read, R. J., Greenhough, T. J., Campbell, J. W., Kalk, K. H., Littlechild, J. A., Watson, H. C. & Hol, W. G. J. (1993). *Proc. Natl Acad. Sci. USA*, **90**, 2355–2359.

Vitkup, D., Petsko, G. & Karplus, M. (1997). *Nat. Struct. Biol.* **4**, 202–208.

Wakatsuki, S. (1993). *Data Collection and Processing*, edited by L. Sawyer, N. W. Isaacs & S. Bailey, pp. 71–79. DL/Sci/R34. Warrington: Daresbury Laboratory.

Weisgerber, S. & Helliwell, J. R. (1993). *J. Chem. Soc. Faraday Trans.* **89**, 2667–2675.

Wilson, A. J. C. (1942). *Nature (London)*, **150**, 151–152.

Wulff, M., Schotte, F., Naylor, G., Bourgeois, D., Moffat, K. & Mourou, G. (1997). *Nucl. Instrum. Methods Phys. Res. A*, **398**, 69–84.

Wyckoff, H. & Richards, F. M. (1967). *J. Mol. Biol.* **27**, 563–578.

Xie, Y. & Hao, Q. (1997). *Acta Cryst.* A**53**, 643–648.

Yang, X. & Moffat, K. (1996). *Structure*, **4**, 837–852.

Yang, X., Ren, Z. & Moffat, K. (1998). *Acta Cryst.* D**54**, 367–377.